Applied Geochemistry 97 (2018) 40–60

Contents lists available at ScienceDirect

Applied Geochemistry

journal homepage: www.elsevier.com/locate/apgeochem

Palaeohydrogeology using geochemical, isotopic and mineralogical analyses: Salinity and redox evolution in a deep groundwater system through Quaternary glacial cycles

Antoni E. Milodowski[a,*], Adrian Bath[b], Simon Norris[c]

[a] British Geological Survey (BGS), Keyworth, Nottinghamshire, NG12 5GG, UK
[b] Intellisci, Loughborough, Leicestershire, LE12 6SZ, UK
[c] Radioactive Waste Management Ltd (RWM), Harwell, Oxfordshire, OX11 0RH, UK

ARTICLE INFO

Editorial handling by Prof. M. Kersten

Keywords:
Palaeohydrogeology
Quaternary
Glaciation
Redox
Salinity
Fracture mineralisation
Secondary calcite
Iron-manganese oxyhydroxide
Cerium
Geological disposal

ABSTRACT

Mineralogical, geochemical and isotopic analyses of secondary calcites are interpreted as part of an investigation of deep groundwaters in fractured metavolcanic rock overlain by sedimentary rock. Drillcore rock samples and groundwater samples from deep boreholes (maximum depth 1950 m) were analysed. This produces information about the evolution of salinity and redox in relation to past groundwater movements including the impacts of climatic change through the Quaternary period.

Salinities of present-day groundwaters vary from dilute to brine concentrations and are related to three distinct groundwater flow regimes. Crystal morphology, stable isotopic analyses and isotopic dating, cathodoluminescence and microanalyses of Fe, Mn and REEs in the latest generation of secondary calcite, plus other analyses, have provided insights into variations of salinity over time and of redox in past groundwaters. Interpretation suggests that groundwater in the depth range of the transition from dilute to brackish/saline concentrations has been gradually diluted over time by meteoric water ingress. $^{230}Th/^{234}U$ whole-crystal ages indicate that at least part of the late-stage calcite mineralisation in the present groundwater flow system is of Quaternary age, although the mineralisation may have been initiated much earlier by meteoric invasion in the Miocene, following regional uplift. The calcites exhibit a wide range in oxygen isotope composition ($\delta^{18}O_{PDB}$ −2 to −22‰), although no extremely light or heavy $\delta^{13}C$ values indicative of microbial methane oxidation or deep methanogenesis were observed. The very light $\delta^{18}O$ values suggest that glacial or other cold-climate waters flowed to more than 700 m depth in the centre of the study area and formed a greater proportion of groundwater at that depth than at present.

Fe and Ce are interpreted as semi-quantitative proxies for past redox conditions over the period when secondary calcite was deposited. Variability of Fe and Mn contents of secondary calcites in deeper rock, presently containing saline groundwater, is evidence of reducing conditions being maintained in the long term, though the strength of negative redox has probably fluctuated due to other redox-active chemistry. Depth-wise changes of groundwater redox in the past are also indicated by Ce concentrations versus other REEs in secondary calcites. Shallow calcites show a negative Ce anomaly in some growth zones due to oxidation to Ce^{IV} whilst deeper calcites do not exhibit this Ce behaviour, indicating that reducing conditions prevailed. Distribution of Fe-Mn oxyhydroxides and pyrite confirm, at a broader scale over depth and time, the findings about redox variations that secondary calcites indicate.

Mineralogical and geochemical studies add further information to the understanding of past geochemical conditions in deep groundwaters in this area. Interpretations provide semi-quantitative constraints on the evolution and likely variations and directions of movement of groundwater salinity and redox over the Quaternary timescale.

* Corresponding author.
E-mail address: aem@bgs.ac.uk (A.E. Milodowski).

https://doi.org/10.1016/j.apgeochem.2018.07.008
Received 10 December 2017; Received in revised form 8 July 2018; Accepted 11 July 2018
Available online 19 July 2018

1. Introduction

Safety assessment of a geological repository typically evaluates containment by the engineered and natural barriers for a reference scenario which assumes that present-day groundwater conditions are in equilibrium and will persist for long times into the future. Potential changes to those conditions are considered in terms of variant scenarios. The credibility of this approach to modelling future repository safety depends on understanding what changes occurred in the past and how the scale of changes might have been influenced by the particular setting. The relevant timescale for safety projections of up to a million years means that changes of climate and sea level at the surface, and neo-tectonic changes within rock formations, might be significant processes. A principle of geological disposal in a repository at hundreds of metres depth is that the impacts of these long-term changes on groundwater conditions are attenuated but cannot be assumed to be insignificant without appropriate analysis.

The best approach to analysing future impacts of scenarios is to study and interpret multiple lines of evidence for impacts on groundwater conditions in the past and present. Present-day groundwater conditions at depth are an artefact of palaeohydrogeological episodes and past climates and may not be related to current boundary conditions. There is a need to allow for hydraulic and chemical disequilibrium in safety assessment analyses.

Palaeohydrogeology covers groundwater movements and compositions, which tend to be coupled. For example, temporal changes of salinity are an indication of transient flows which may be caused by climate-driven changes of hydraulic conditions. An important property of groundwater in regard to the safety of radioactive waste disposal is redox. Redox is sensitive to transient groundwater flows because of the effect on redox of the ingress of dissolved oxygen. In general, changes to the driving force and/or direction of groundwater movement are likely to disturb the geochemical steady state for water-rock reactions that control redox, pH and reactive solutes. Of particular concern is the potential impact that the sub-glacial recharge of meltwater may have in future on redox conditions at repository depth. Glacial meltwaters are expected to contain much higher concentrations of dissolved oxygen than would be present in cold, dilute water equilibrated with the atmosphere due to the trapping of air in snow during its deposition, and which subsequently remains trapped when the snow is transformed to ice during burial and compaction within glaciers (e.g. Stauffer et al., 1985; Souchez et al., 1995). The oxygen remains dissolved in the subglacial meltwater because of the elevated pressure beneath the melting ice (Guimerà et al., 1999). The penetration of oxidising groundwater to repository depth would enhance the corrosion of waste canister materials (e.g. steel or copper), thereby impacting on the long-term performance of the engineered barrier. In addition, redox-sensitive radionuclides may be more mobile as oxidised species. The objective of this palaeohydrogeological study is to evaluate the evidence that groundwater systems become less influenced by the impacts of climate change with increasing depth below the geosphere-biosphere surface. Results and conclusions presented here are inevitably site-specific and might not be applicable in other geological settings, however the methods used here and their evaluation are of general interest for investigations in low permeability rocks and aquifers.

2. Geological and hydrogeological setting

2.1. Bedrock geology

The study area is situated adjacent to the nuclear site at Sellafield on the lowlands of the coastal plain of west Cumbria, in north-west England. These lowlands have an average elevation of < 100 m above sea level (Ordinary Datum, OD) in this part of west Cumbria (Heathcote and Michie, 2004). The regional geology of the area has been described in detail by Nirex (1997a), Michie and Bowden (1994), Michie (1996), Akhurst et al. (1997) and Heathcote and Michie (2004) and is summarised in Fig. 1. It is situated in the transitional structural zone between the western margin of the Lake District Massif comprised largely of Lower Palaeozoic rocks, and the largely offshore East Irish Sea Basin, which contains younger (Carboniferous, Permian and Triassic) sedimentary strata. To the east, the area is bounded by Ordovician to Silurian igneous and low-grade (greenschist facies) metamorphic rocks which form the Cumbrian Mountains, rising to over 800 m within 15 km of the present-day coast. The same rocks form the crystalline basement that underlies the Carboniferous and Permo-Triassic sedimentary sequence in the study area. The top of the basement comprises Borrowdale Volcanic Group (BVG) metavolcaniclastic rocks.

Boreholes were drilled and cored to a maximum depth of 1950 m in an area of about 20 km^2 in the 1990s by United Kingdom Nirex Limited ('Nirex') (Fig. 1). In the centre, the basement is at a depth of approximately 500 m and is overlain by Carboniferous and Permo-Triassic sedimentary strata. The Carboniferous rocks are represented by a thin sequence of Dinantian (Carboniferous Limestone) shallow marine limestones with thin shale interbeds that rest unconformably on the eroded basement surface. These strata attain a maximum thickness of about 300 m and outcrop to the north of the study area. However, within the study area they thin eastwards to a feather edge under a cover of Permo-Triassic sandstones about 1 km inland of the coast (Barclay et al., 1994; Akhurst et al., 1997), and are encountered only in the deep boreholes in the centre of the area and near to the coast. Permo-Triassic strata rest unconformably on the Carboniferous rocks, forming a wedge overlapping onto the BVG basement to the east, and their outcrop delineates the north-eastern margin of the major Mesozoic East Irish Sea Basin (Colter and Barr, 1975; Fletcher and Ransome, 1978). A diachronous sedimentary breccia up to 70 m thick of Permian age, the Brockram formation, marks the base of the Permo-Triassic sedimentary sequence. In the west, this basal breccia rests on the Carboniferous, and passes upwards and laterally westwards into, the anhydritic and dolomitic St Bees Evaporite and St Bees Shale formations. In turn, the St Bees Shale is overlain by the Triassic Sherwood Sandstone Group: a sequence of sheet-flood, fluvial and aeolian sandstones and siltstones, with thin mudstones. In the east, the Brockram formation rests on the BVG and passes upwards directly into the Sherwood Sandstone Group. The sandstones are up to 1000 m thick, thinning from offshore to onshore, and contain an aquifer in the more permeable upper part. Offshore, they are overlain by a thick sequence of mudstones and evaporites (including halite) belonging to the Triassic Mercia Mudstone Group. The coastal lowlands are blanketed by a varied sequence of unconsolidated Pleistocene glaciofluvial and glaciolacustrine deposits overlying the top of the sandstones. These are largely of Devensian age, although pockets of pre-Devensian deposits are preserved locally (Akhurst et al., 1997; Heathcote and Michie, 2004).

2.2. Groundwater

External features that are likely to have a substantial influence on groundwater movements at depth in the study area are: (a) the topographic gradient between the Cumbrian mountains and coastal plain over around 15 km distance; (b) the proximity of an offshore sedimentary basin containing sandstones and bedded evaporite deposits; and (c) spatial variation of surficial rock types, with varying permeabilities, from inland basement rocks to sandstones overlain by glacial deposits in the coastal plain.

Three distinct hydrogeological domains exist in the basement rocks and sedimentary cover rocks of the coastal lowlands in this area of west Cumbria (Black and Brightman, 1996). These are: (a) the 'Coastal Plain Regime' in which groundwater flow is topographically driven with boundaries determined by the position of the coast and extent of surficial transmissive rocks; (b) the 'Irish Sea Basin Regime' in which flow at more than 600 m depth under the coast and offshore is driven by

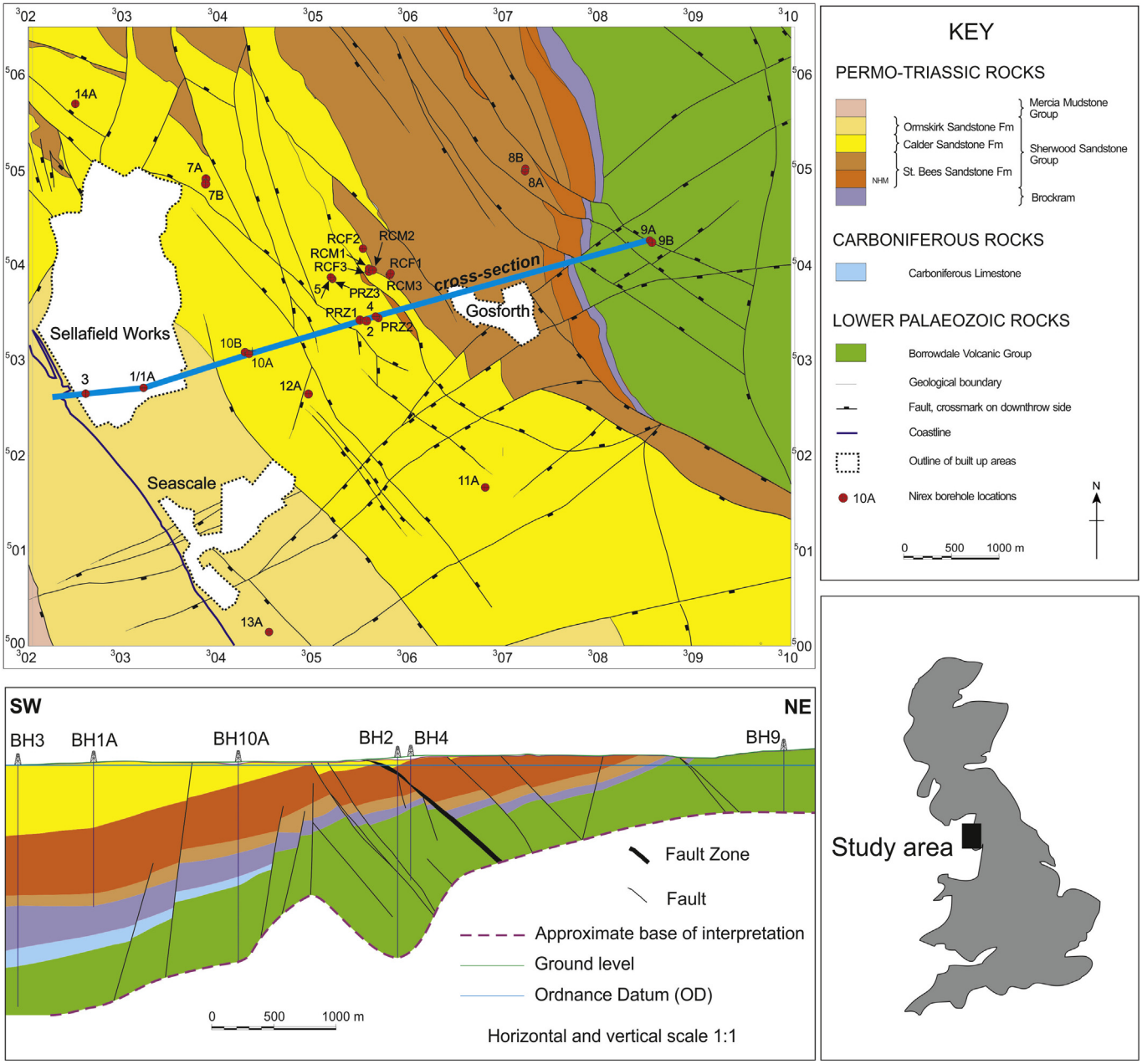

Fig. 1. Geological map of west Cumbria with simplified geological cross-section drawn along an east-west profile.

processes in the basin; and (c) the 'Hills and Basement Regime' in which flow is likely to be relatively slow and is largely driven by topography but also by other factors such as variations of water density due to increasing salinity which may be significant at greater depth.

Salinities of groundwaters are categorised in terms of total dissolved solids (TDS): fresh < 1000 mg/L; brackish ≥1000 to < 10,000 mg/L; saline ≥10,000 to < 100,000 mg/L; brines ≥100,000 mg/L.

Chemical and isotopic compositions of groundwaters, based on analyses of fifty-seven water samples taken from the deep boreholes (Fig. 1), are summarised in Table 1. Data for these samples have been selected from a much larger data set on the basis that contamination from drilling fluids was minimised and data are considered to be representative of in situ compositions except for Eh and carbon isotope measurements. Data for major solute chemistry, stable isotopes, strontium isotopes and dissolved gases in individual water samples can be found in Bath et al. (2006). Three chemically- and isotopically-distinct groundwater types are identified in the groundwaters: fresh and brackish groundwaters that change from Ca-HCO_3 with water stable isotope ratios ($^{18}O/^{16}O$ and $^{2}H/^{1}H$) similar to local precipitation to Na-Cl compositions with lighter stable isotope ratios as salinity increases; brines that have Na-Cl compositions with Ca and SO_4 as secondary components and heavier stable isotope ratios; and saline groundwaters that are chemically distinct from brines in terms of higher Ca/Na, K/Na, SO_4/Cl, Br/Cl and $^{87}Sr/^{86}Sr$ and also have lighter stable isotope ratios characteristic of cold climate water (Bath et al., 1996, 2006). Br/Cl ratios in the saline groundwaters are higher than in the brines, showing that their compositions are not simply the result of dilution of brines but have had Br and other solutes added from reactions in the basement rocks.

$^{87}Sr/^{86}Sr$ ratios are highest in saline groundwaters in basement covered by sedimentary rocks (Table 1). The same groundwaters have higher Br/Cl ratios. High Sr isotope ratios and high Br/Cl indicate a greater extent of water-rock reaction and long residence times for these basement saline groundwaters (Bath et al., 2006). Lower $^{87}Sr/^{86}Sr$

Table 1
Summary of groundwater compositions in deep boreholes at Sellafield, West Cumbria. More detailed listing of chemical, isotopic and dissolved gas compositions of individual water samples are given in Bath et al. (2006). 'm OD' = metres relative to Ordinary Datum, i.e. sea level. Lithologies are: SSG = Sherwood Sandstone Group, BVG = Borrowdale Volcanics Group, CL = Carboniferous Limestone, BrkB = Brockram breccia formation, SBEv = St Bees Evaporite formation.

Borehole	Depth	Lithol	pH	TDS	Major ions	Ca^{2+}	Mg^{2+}	SO_4^{2-}	HCO_3	Fe	Mn	HS^-	Ce	$\delta^{18}O$	$^{87}Sr/^{86}Sr$
	m OD			mg/L		mg/L							µg/L	‰	
2	−146 to −296	SSG	7.25–8.26	165–259	Ca-Na-HCO_3	12–33	4–15	7–17	124–200	0.01–0.03	0.06–0.11		< 0.3	−6.0 to −6.1	
2	−650 to −1525	BVG	6.52–8.74	21900–30200	Na-Cl	484–1550	62–162	962–1210	8–185	2.3–8.17	1.88–2.07	nd-0.1	< 15–25.9	−7.5 to −8.0	0.714648–0.715200
3	−679 to −1096	SSG	7.22–7.79	113000–188000	Na-Cl	2270–2520	465–686	3580–4910	16–55	6	2.54	nd	< 30-138	−6.3 to −5.1	0.710062–0.714531
3	−1530	CL	6.47	135000	Na-Cl	2610	537	4740	184					−5.8	0.711258
3	−1659	BVG	7.31	177000	Na-Cl	2910	489	3340	< 5					−5.9	
4	−347 to −733	BVG	7.73–8.20	2460–24000	Na-Cl	16–867	2–105	151–1110	31–355	2.5–3.88	1.6–1.82	nd	< 30	−6.5 to −7.6	
7A	−503	CL	7.50	30400	Na-Cl	1500	202	840	68					−7.4	
7A	−833	BVG	7.65	67600	Na-Cl	1970	239	1500	79					−7.0	
8A	−790	BVG	7.89	17500	Na-Cl	534	80	793	50					−7.1	
9A&9B	+41 to −369	BVG	7.89–8.29	1680–20100	Na-Cl	55–828	13–130	61–889		0.09–12.4	0.19–1.61	nd-0.1		−6.3 to −7.6	0.711939–0.714562
10A	−560	SSG	7.88	722	Na-Cl	33	47	51	261					−6.7 to −7.5	0.716452
10A	−925	CL	7.45	65100	Na-Cl	1950	274	1920	41	4.71	2.28	0.3		−7.2	0.713783
10A	−1033 to −1558	BVG	6.67–7.96	84900–135000	Na-Cl	2240–2810	320–424	1810–3420	45–116					−6.3 to −6.9	0.712432–0.713408
11A	−719	SSG	7.65	17000	Na-Cl	993	123	970	45	15.9	1.8	nd		−7.6	
11A	−830	BrkB	7.53		Na-Cl	1070	96	972	123					−7.9	
11A	−945	BVG	7.79	21000–21600	Na-Cl	1390	114	996	8	11.8	1.48	nd		−7.9 to −8.1	
12A	−533	SSG	7.90	561	Na-HCO_3-Cl	13	21	24	280	0.1	0.29	nd		−6.5	
12A	−526	BrkB	7.83	50800	Na-Cl	1810	225	1810	< 5					−7.4	
12A	−963 to −1069	BVG	8.10	67700–68000	Na-Cl	2450–2680	292–340	1830–1940	< 5-15	12.7–13.6	2.8–3.49	nd		−7.1 to −7.4	
13A	−1440	SBEv	7.86	142000	Na-Cl	2540	635	4720	48	6.15	1.9	0.1		−6.0	
PRZ2	−300	SSG	8.00–8.59	286–287	Na-HCO_3-Cl	30	10	10		0.08–0.16	0.06–0.16	nd		−6.3	
PRZ2	−327	BrkB	8.40	2010	Na-Cl	24	3	137		0.06	0.20	0.1		−6.5	
PRZ2	−425	BVG	7.30–7.81	21500	Na-Cl	1280–1303	114–116	994–1050		3.68	1.56	nd		−7.5	
PRZ3	−396 to −445	BrkB	8.26	3730–17600	Na-Cl	51–646	8–85	218–747						−6.8	
RCF1	−341	BrkB	7.73	17900	Na-Cl	516	61	720						−7.3	
RCF2	−694	BVG	7.87	24600	Na-Cl	1160	146	1070						−7.9	
RCF3	−302	SSG	8.34	289	Na-HCO_3-Cl									−6.1	

ratios in groundwaters in sedimentary cover rocks, especially in deep brines in the thick sedimentary sequence below the coast, can be explained by the lower production of radiogenic ^{87}Sr in sandstones and in offshore evaporites from which the brines derive their high salinity.

Fresh-brackish groundwaters occur predominantly in the sandstone aquifer and in the shallowest, weathered, part of outcropping basement rocks at the eastern edge of the area, i.e. in the coastal plain flow regime. The vertical extent of brackish groundwater is rather limited. Over most of the area, the base of fresh water is only a few tens of metres above the shallowest occurrence of saline groundwater.

Brine groundwaters have been found in the deep sedimentary rocks where they thicken westwards into the Irish Sea Basin and in underlying basement rocks. These groundwaters are referred to as 'basinal brines'.

Saline groundwaters dominantly occur in the basement in the centre and eastern parts of the area, i.e. the hills and basement flow regime, and are referred to here as 'basement saline groundwaters'. Saline groundwaters also occur at depth, overlying brine, in the sandstone and the basal sedimentary formations in the western, coastal part of the area. Brackish and saline waters were sampled in the sandstone formation near the coast.

The three groundwater types – fresh-brackish, basinal brine and basement saline – are closely related to the three hydrogeological regimes because of the general relationship between relatively low flow velocities and retention of salinity in a deep groundwater system. Mixing of the groundwater types occurs at the interfaces between the flow regimes.

The spatial distribution of chemically-distinct groundwaters has both direct and indirect significance to understanding present and past groundwater movements. It has direct significance because of the influence of density variation on hydraulic gradients and hydrodynamics. Large contrasts in groundwater density inhibit flow, with solutes being exchanged across a broad mixing zone by diffusion and dispersion. The distribution of water types has indirect significance because the origins and mixing of water and solutes are evidence of directions and timing of groundwaters movements in the past.

Groundwater residence times have been estimated from stable water isotope ratios and chlorine-36 measurements (Bath et al., 2006; Metcalfe et al., 2007). Carbon-14 data were mostly unreliable because of contamination of samples by drilling fluid (Bath et al., 2006). Residence times for groundwaters correlate with their widely-varying salinities and with the distinct hydrogeological domains. Dilute groundwaters in the sandstone of the Coastal Plan regime are all of post-glacial Holocene age, < 10 ka.

Brackish and saline groundwaters, at the base of the sandstone in the centre of the area below 500–600 m and in the underlying breccia and basement have relatively light stable isotope ratios typical of cold climate recharge and have Pleistocene ages, > 10 ka. These groundwaters are in the Hills and Basement regime. The stable isotope ratios indicate that the water originated as meteoric infiltration in both glacial and interglacial periods, although water with very light isotopic ratio indicative of glacial melt water has not persisted presumably because of dispersion and mixing. Pleistocene-age water has flowed to greatest depth, around 800–900 m depth, in the thickening sedimentary rock between the centre of the area and the coast.

Groundwaters in the Hills and Basement regime have become saline due to mixing with older and deeper saline groundwater during slow groundwater movement from east to west (Black and Brightman, 1996; Nirex, 1997a). There are two sources of salinity: one in the inland basement rocks and the other as brines in the offshore Irish Sea Basin regime where evaporites occur in the sedimentary sequence. Chlorine-36 data indicate that brine groundwaters under the coast at the western boundary of the study area have residence times > 1.5 Ma (Metcalfe et al., 2007).

Hydraulic testing in the deep boreholes produced depth profiles of groundwater pressures that showed a peak of environmental heads at around 1100 m after adjusting the pressures for the increasing salinity-density with depth and for local water table elevation (Black and Barker, 2015). The anomalously high heads extend for several hundred metres above and below the peak where tests were made in the BVG basement. This feature of groundwaters in the basement rocks has been interpreted as a likely relic of high groundwater pressures caused by an overlying wet-based ice sheet during the last Pleistocene (Devensian) glaciation of this region (Black and Barker, 2015). Modelling indicates that relic pressures would be preserved only if the hydraulic diffusivity of these rocks is in the order of $10^{-6}\,m^2\,s^{-1}$, i.e. consistent with very low permeability. Alternative possible interpretations for the high heads include lateral hydraulic gradients due to the salinity-density contrast between brines to the west under the coast and saline groundwaters and geothermal convection due to high heat flow, but these explanations have been discounted in favour of relic sub-glacial pressure (Black and Barker, 2015).

2.3. Quaternary climate history

Britain was affected by multiple glaciations during the Pleistocene and onshore four principal glaciations are recognised: the Loch Lomond Stadial (or Younger Dryas, c.10–11 ka); preceded by the main Late Devensian (Weichselian) glaciation (26-13 ka) which left a marked imprint on the landscape across Britain; in turn preceded by the Wolstonian (186-128 ka BP) and Anglian (ca. 480-430 kyr BP) glaciations (Clarke et al., 2004; McEvoy et al., 2016). Details of the Quaternary chronostratigraphy and climate states for west Cumbria have been described previously (Akhurst et al., 1997; Heathcote and Michie, 2004) and a summary is provided in Supplementary Table 1.

Glaciation prevailed for about 100 ka of the last 700 ka, and periglacial conditions with permafrost dominated for about 200 ka over that period. The most recent (Devensian) glacial stage lasted about 116 ka, about 20% of which involved full ice cover, and ended at about 10–13 ka ago. Conditions during the other glacial stages in the Pleistocene might have been similar, though the evidence of their extent and severity is sparse. Climate variations during the Quaternary would have caused fluctuations in the amount of fresh water recharge. In interglacial periods, it is assumed that topographically-driven groundwater flow would have restarted, except where permafrost inhibited recharge through the ground surface.

2.4. Fracture and fracture mineralisation history

The fracture mineralogy and paragenesis of west Cumbria was studied in detail as part of the Nirex site investigation programme at Sellafield (Milodowski et al., 1995, 1998; 2002, and references therein). These studies established that the basement and overlying sedimentary cover rocks within the present study area have experienced a long and complex history of fracturing, fluid movement and fracture mineralisation. A series of broad but distinctive 'Mineralisation Episodes' (referred to as 'ME1' [the oldest] to 'ME9' [the youngest]) have been distinguished (Milodowski et al., 1998, 2002; Bouch et al., 2004), and is summarised in Table 2.

ME1 to ME3 occur only in the BVG-hosted fractures and comprise silicate-dominated mineralisation (with subordinate sulphides) related to moderately high-temperature (epithermal to mesothermal) low-to moderate-salinity hydrothermal fluid circulation. Low-temperature hydrothermal mineralisation (CME1) dominated by calcite and specular hematite (± siderite and manganese oxides) occurs in both the BVG basement and Carboniferous Limestone. ME6 to ME7 affect the BVG, Carboniferous and Permo-Triassic rocks, and correlate with the burial diagenesis of the Permo-Triassic sedimentary strata (Milodowski et al., 1998; Nirex, 1998a).

ME8 and ME9 mineralisation affect the BVG, Carboniferous and Permo-Triassic rocks, and are closely associated with present-day groundwater flow in the deep site investigation boreholes in the study

Table 2
Summary of the paragenesis, principal mineral assemblages and stratigraphical range of fracture mineralisation in the Nirex site deep boreholes in west Cumbria.

Mineralisation Episode (ME)	Principal mineral assemblage	Inferred age/origin
Affects the BVG basement only		
ME1	Quartz ± albite ± K-feldspar (adularia) ± chlorite ± hematite	*Lower Palaeozoic:*. Related to mid-Devonian moderate-high temperature (epithermal-mesothermal) hydrothermal circulation within BVG.
ME2	Quartz ± epidote ± calcite ± chlorite ± actinolite ± apatite ± K-feldspar ± albite ± sericite ± hematite	*Upper Palaeozoic (pre-Carboniferous):* Moderate to high-temperature (109–300 °C) epithermal mineralisation by low- to moderate salinity (0.2–11.5 wt % eq. NaCl) associated with late Caledonian Lake District Batholith. Approx. 390-310 Ma.
ME3	Pyrite ± minor to trace chalcopyrite ± arsenopyrite ± pyrrhotite ± marcasite ± galena	*Upper Palaeozoic (pre-Carboniferous):* Epithermal mineralisation closely associated with late stage of ME2
Affects the BVG basement and Carboniferous Limestone strata. Not present in the Permo-Triassic strata		
CME1[a]	Calcite ± siderite ± specular hematite ± Mn oxides	*Late Carboniferous-Early Permian:* Low temperature hydrothermal mineralisation pre-dating the Permian unconformity. In part, possibly related to Permian weathering.
Affects BVG basement to Permo-Triassic strata		
ME4	Major anhydrite ± minor to trace barite ± fluorite ± hematite ± quartz ± siderite (?)	*Post-Permian or syn-Triassic:* Anhydrite derived from remobilization of Permian evaporites
ME5	Kaolinite ± illite ± albite ± K-feldspar ± hematite	*Mid-Triassic to ?Early Jurassic:* Mineralisation by warm basinal brines evolved during burial diagenesis of Carboniferous and Permo-Triassic strata in the East Irish Sea Basin. Closely associated with ME6 and correlated with late burial diagenetic cements in the Brockram. *[not evident in the Carboniferous Limestone]*
ME6a[b]	Major calcite and colloform-earthy hematite	*Mid-Triassic-?Early Jurassic:* Hydrothermal mineralisation associated with expulsion of warm (50–180 °C), Na-Ca-Cl-SO_4-brines (up to 25 wt% equivalent NaCl) from the East Irish Sea Basin during deep burial and diagenesis of the evaporite-bearing Permo-Triassic sedimentary fill.
ME6b	Major dolomite, ferroan dolomite, ankerite, anhydrite ± minor to trace siderite ± quartz	
ME6c	Major calcite ± minor to trace barite ± fluorite ± hematite ± pyrite ± chalcopyrite ± sphalerite ± galena ± Ag-, Ag-Bi, Bi-selenides ± quartz ± rare uranium minerals	
ME7	Illite ± hematite	*Mid-Triassic – Early Cretaceous:* Alteration associated with major fault movements.
Affects BVG basement to Permo-Triassic strata: closely associated with present-day groundwater flow		
ME8[c]	Mn- and Fe oxides/oxyhydroxides.	*?Late-Tertiary to Quaternary:* Oxidative alteration, and dissolution of carbonate and anhydrite mineralisation following uplift, weathering and meteoric invasion. Associated with modern shallow groundwater system
ME9[c]	Calcite ± pyrite ± marcasite ± anhydrite ± gypsum ± barite	*?Late-Tertiary – Quaternary:* Mineralisation closely associated with modern deeper groundwater system.

Notes:
[a] Originally defined as 'Early ME6a' Permo-Triassic mineralisation (Milodowski et al., 1998, 2002) but now recognised as pre-dating the Permian unconformity at Sellafield and revised as a separate Carboniferous Mineralisation Episode 'CME1' (Bouch et al., 2004).
[b] Originally defined by Milodowski et al. (1998, 2002) as 'Late ME6a', now referred to simply as 'ME6a'.
[c] ME8 and ME9 may be coeval in part, with ME8 occurring near-surface simultaneously with ME9 mineralisation in deeper parts of the groundwater system.

area. ME8 is represented by iron and manganese oxyhydroxides formed by the oxidative dissolution and alteration of earlier ferroan carbonate and sulphide vein mineralisation and cements and is found in the shallow groundwater system. ME9 is dominated by calcite sometimes accompanied by minor to trace amounts of pyrite, marcasite, anhydrite, gypsum and barite. This late-stage mineralisation is the focus of this present study.

Further information on textural relationships between the different generations of carbonate mineralisation are summarised in the schematic illustration and example images provided in the Supplementary Figures.

3. Investigation methods

3.1. Groundwater sampling and analyses

Details of the drilling conditions, hydraulic testing and sampling of boreholes are reported in Nirex (1997b). Most of the groundwater samples used in this study were obtained by discrete extraction tests (DETs) carried out either during drilling or after borehole completion. Depth intervals between 8 and 50 m long, mostly 10–20 m, were isolated by packers and were pumped either by nitrogen gas lift or by submersible pump. A chemical tracer, usually Li^+, was added to drilling water so that contamination of water samples could be quantified. Water samples for which compositions are used in this study mostly had < 5% introduced drilling water. Details of sample treatment, analyses and data processing to estimate in situ values for major solute concentrations and TDS (total dissolved solids) are in Bath et al. (1996, 2006). Stable O and H isotopes, and Sr isotope ratios were analysed by conventional mass spectrometry. Concentrations of total iron (Fe) and manganese (Mn) were measured by ICP-OES. Rare earth elements (REEs) in a subset of water samples were analysed by inductively coupled plasma mass spectrometry (ICP-MS) (Nirex, 1998b). Detection limits for REEs varied, depending on the widely varying TDS contents of water samples. Effects of drilling fluid contamination on trace element contents were negligible and values were not adjusted as had been done for the major solutes.

3.2. Petrological characterisation of late stage (ME8 and ME9) fracture mineralisation

3.2.1. Distribution of fracture mineralisation

Mineralogical analyses undertaken during the Nirex site investigations at Sellafield identified definitive characteristics that allowed the different MEs in fracture mineralisation to be recognised in hand specimen (Milodowski et al., 1995, 1998). Using these characteristics, systematic borehole core logging was undertaken to evaluate the nature and spatial distribution of vein mineralisation associated with potential flowing features (PFFs) correlated with groundwater inflows ("flow-zones") identified by geophysical and hydrogeological logging in the boreholes (Nirex, 1997c). A simple stereoscopic binocular microscope, together with staining of selected carbonate mineralisation (Dickson, 1966), was used to record details of fracture surfaces, vein fabrics and mineral morphological characteristics from over 37,000 fractures from

18 deep boreholes (Milodowski et al., 1997, 2002).

3.2.2. Mineralogical and geochemical analysis

Detailed observations and analyses were made on 135 samples of ME9 calcite mineralisation (Supplementary Table S2). High-resolution petrographic analysis of polished sections was undertaken using optical microscopy, cold-cathodoluminescence microscopy (CL) and back-scattered scanning electron microscopy (BSEM) supported by energy-dispersive X-ray microanalysis (EDXA). Calcite morphology was examined by optical binocular and scanning electron microscope (SEM) using secondary electron imaging (SEI). Major and trace element analyses of a representative subset of calcite were determined by wavelength-dispersive or energy-dispersive electron probe microanalysis (EPMA), and laser ablation microprobe inductively-coupled plasma mass spectrometry (LA-ICPMS).

Microthermometric measurements of fluid inclusions (temperatures of homogenisation (T_h), first ice-melting (T_{fm}) and final ice-melting (T_{ice})) were recorded from 57 samples of ME9 calcite. Salinities were calculated from ice-melting data using "CalcBrine 1.5" (Naden, 1996), which allows calculation of salinities in the binary systems NaCl-H_2O, $CaCl_2$-H_2O and in the ternary system NaCl-$CaCl_2$-H_2O. Where first melting data were available to characterise the components present in the fluid, the appropriate binary or ternary system was considered. Calculation of NaCl: $CaCl_2$ ratios requires measurement of the salt-hydrate melting temperature (T_{hyd}), but since this could not be determined in these samples the salinity was calculated as equivalent wt. % NaCl. Fluid inclusion chemistry (Na, Mg, Li, Sr, Fe and Mn) was also determined by LA-ICPMS, using the methodology described by Milodowski et al. (2005), on 40 fluid inclusions from a very limited subset of 9 ME9 calcites which had large enough inclusions. Inevitably, the laser ablation of the fluid inclusions included some contamination ablated from the host calcite. To correct for this, complementary element concentrations were obtained from the adjacent host calcite, and then subtracted from the raw fluid inclusion LA-ICPMS data, after normalising to the fluid inclusion Ca value (assuming that all the Ca present in fluid inclusion analyses was contributed from the calcite host). The resulting values were reported as 'matrix-corrected' arbitrary concentration units ('acu' mass units), although there are substantial uncertainties in these data (Bath et al., 2000).

Stable ($\delta^{13}C$ and $\delta^{18}O$) isotope analyses and strontium isotope ratio ($^{87}Sr/^{86}Sr$) analyses of bulk ME9 calcite crystals and other generations of carbonate mineralisation have been reported previously (Milodowski et al., 1998 and references therein). A small suite of 7 samples of ME9 calcite crystals have subsequently been analysed for $\delta^{13}C$ and $\delta^{18}O$ using a He-flushed laser ablation carbonate-extraction (He-LACE) micro-sampling system or diamond microdrill to try to sample individual calcite growth zones. Calcite crystal were mounted either in gypsum plaster or low melting point (70 °C) M70 alloy, rather than epoxy-resin to avoid contamination from resin ablation. The samples were selected to be representative of ME9 calcite from the freshwater and saline groundwater zones.

Ten ME9 calcites and 2 samples of ME8 manganese oxyhydroxide were previously dated as part of a separate study to constrain the timing of fault movement in west Cumbria (Nirex, 1998a). The calcite was dated by the $^{230}Th/^{234}U$ method using alpha spectrometry or high-resolution inductively-coupled plasma mass spectrometry (HRICPMS), or by thermal ionisation mass spectrometry (TIMS). Pure calcite crystals carefully hand-picked from fracture surfaces under a binocular microscope. Because of the very low uranium content of these calcites (typically < 0.1 ppm U) a significant amount of material (100–500 mg) was required to provide sufficient U for analysis. Therefore, "whole crystals" rather than from individual growth zones were analysed. However, since ME9 calcite is often nucleated upon cores of old ME6 carbonates, the sampling focused on breaking off the tips and edges of the ME9 calcite overgrowths to try to avoid the older core material. Consequently, the dates are biased towards the younger outer parts of these calcite crystals. Seven calcite samples were also submitted for ^{14}C determination by accelerator mass spectrometry (AMS). The manganese oxyhydroxide material was dated by ^{40}Ar-^{39}Ar method, using: (i) a single-step laser fusion argon extraction technique on small clusters of grains, and; (ii) incremental heating extraction of large samples (30–60 mg) in a double-vacuum resistance furnace. This method has been applied to date manganese oxyhydroxides (which often incorporate a small potassium component) in ancient weathering profiles (Vasconcelos et al., 1994).

4. Results

4.1. Dissolved iron, manganese and rare earth elements

Only analyses of Fe and Mn in water samples with the lowest degrees of drilling water tracer content, < 1%, are reported (Table 1). Dissolved Fe ranges from 0.01 to 16 mg/L; Mn ranges from 0.1 to 3.5 mg/L. Fe concentrations are < 0.2 mg/L in water samples from above 420 m depth and are almost all > 2 mg/L at greater depths. Some water samples had relatively high contents of dissolved Fe, > 1 mg/L. Samples with < 0.2 mg/L Fe have TDS values that are < 3500 mg/L, and conversely those with > 1 mg/L Fe have much higher TDS values. It is inferred that the high contents of Fe in saline and brine groundwaters are stabilised by complexing with chloride and sulphate. Similarly, the variations of dissolved Mn are attributed to complexation in groundwaters with higher salinities. Mn concentrations also increase with depth and are correlated with salinity with concentrations being > 1.5 mg/L when TDS is greater than 20,000 mg/L.

Rare earth elements were analysed in a limited number of samples. Detection limits increased with salinity due to solution matrix effects. Analyses of La, Pr, Nd, Sm, Eu, Gd, Dy, Er, Yb and Lu were all below detection limits. Only analyses of Ce in some samples were significantly above detection limit (Table 1). With one exception, these were saline water samples from basement rock.

4.2. The occurrence and distribution of late stage ME8 and ME9 fracture mineralisation

The distribution of ME8 and ME9 mineralisation was studied in detail during the site investigations (Milodowski et al., 1995, 1997, 1998, 2002). ME8 is characterised by amorphous, cryptocrystalline and microcrystalline black to dark brown manganese oxyhydroxide, yellow-orange-brown iron oxyhydroxides, and more complex Ba-K-Ca-Mn oxyhydroxides. These secondary oxides occur as thin films, dendritic coatings, encrustations and impregnations staining fracture surfaces and locally impregnating bedding planes and matrix porosity in the upper part of the Sherwood Sandstone Group sandstone aquifer. It also occurs on open fracture surfaces in the shallow BVG (borehole 9A) in the east of the area. These oxyhydroxides precipitated during oxidative dissolution of earlier ME2 and ME6 ferro-manganoan calcite, dolomite and ankerite host rock cements and vein mineralisation, and by alteration of iron and manganese minerals in the host rock matrix and is typical of supergene (near-surface) alteration. ME8 occurs to a maximum depth of about 150 m in borehole 8B and 25 m in borehole 9A in the east, increasing to between 270 and 440 m in boreholes in the centre of the study area. However, it extends to much greater depth (up to about 670 m) in boreholes 10A and 12A. The limit of its vertical extent in the centre of the study area and in boreholes 10A and 12A coincides closely with the base of the freshwater zone in the sandstone aquifer.

ME9 calcite is dominated by euhedral calcite crystals ranging from less than 5 μm up to 20 mm in size, which typically line open fractures. It also occurs as an equivalent diagenetic cement (Milodowski et al., 1998) precipitated within the intergranular porosity in the St Bees Sandstone Formation and in large vuggy cavities in low-matrix breccia horizons in the Brockram. ME9 calcite post-dates ME8, and at shallow

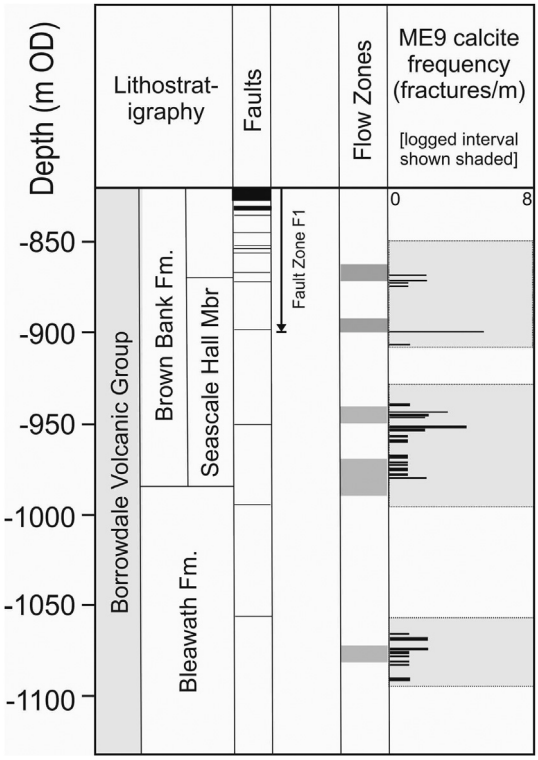

Fig. 2. Example log showing the distribution of ME9 calcite fracture mineralisation and its relationship to faults and flow zones identified by hydrogeological testing. Recorded from a selected interval in the Borrowdale Volcanic Group from Borehole 2 (data from Milodowski et al., 1997; Nirex, 1997b,c).

depths in the sandstone can sometimes be found resting on, and containing inclusions of, ME8 oxyhydroxide mineralisation. The calcite is characteristically translucent, clear, pale brown or reddish in colour, often forming doubly-terminated euhedral crystals. It is commonly developed as syntaxial overgrowths and encrustations on earlier (ME6) calcite, where earlier veins have been reactivated by tectonic processes, or where the dissolution of earlier fracture minerals (usually ME4 and ME6b anhydrite and/or dolomite (cf. Table 2) has created secondary porosity. The preservation of corroded relict cores of ME6 calcite within the ME9 calcite is common, and the presence of euhedral mouldic cavities after tabular anhydrite and rhombic dolomite crystals within the reactivated ME6 carbonate veins, provides evidence that a significant proportion of the present-day fracture porosity is of secondary (mineral dissolution) origin: a feature that is more commonly recognised in sandstone diagenesis (cf. Schmidt and McDonald, 1979).

Fine grained pyrite or marcasite are sometimes associated with the ME9 calcite, as coatings on some unsealed fractures in the deeper parts of the St Bees Sandstone Formation and in many of the open BVG-hosted fractures. In addition, euhedral crystals of anhydrite, gypsum or barite may also accompany ME9 calcite, and appear to be coeval. ME9 anhydrite and gypsum are rare in the east of the study area but are more common in the west of the area (boreholes 3 and 11). In borehole 3, ME9 calcite gradually disappears (or is only very locally developed) in the St Bees Sandstone between −946 and −1044 m OD, giving way below this depth to anhydrite and gypsum in the Carboniferous and BVG strata.

ME9 anhydrite may be derived through the dissolution, mobilisation and re-precipitation of earlier anhydrite. Potential sources include: anhydrite-bearing sedimentary evaporites in the St Bees Shale Formation and St Bees Evaporite (Permian) and Mercia Mudstone Group (Upper Triassic) (Akhurst et al., 1997); anhydrite beds in offshore Carboniferous strata (Crowley et al., 1997), and/or; earlier ME4 and ME6b anhydrite fracture mineralisation, and diagenetic anhydrite cement in the Permo-Triassic rocks. Two samples of pure ME9 anhydrite crystals analysed from the Carboniferous Limestone in borehole 3 (Supplementary Table S5) gave $^{87}Sr/^{86}Sr$ ratios of 0.71086–0.71109, which is similar to the present groundwater ($^{87}Sr/^{86}Sr$ = 0.71126) sampled close by in the same borehole (Table 1). This is significantly more radiogenic than either ME4 anhydrite (Milodowski et al., 1998), anhydrite from the overlying Permian evaporite strata ($^{87}Sr/^{86}Sr$ = 0.70852–0.71000 - Supplementary Table S5), or that expected for marine Carboniferous or Triassic evaporites (McArthur et al., 2001; Korte et al., 2003). However, the $^{87}Sr/^{86}Sr$ ratio of ME9 anhydrite lies within the range reported for ME6b and ME6c calcite, dolomite and anhydrite ($^{87}Sr/^{86}Sr$ = ~0.7090 - ~0.714, Milodowski et al., 1998). Consequently, ME9 anhydrite is most probably sourced through the dissolution and redistribution of earlier ME6b anhydrite mineralisation (with minor contributions from other sources) by groundwater percolation from the east. ME9 anhydrite reprecipitates down-flow in the west as the groundwaters become progressively more concentrated with depth. This is consistent with the observed mouldic dissolution porosity after ME6b anhydrite in fractures to the east, and with the dissolution of diagenetic anhydrite cements observed at shallower levels in the overlying Permo-Triassic rocks (Strong et al., 1994).

The distribution of ME8 and ME9 fracture mineralisation shows a close relationship to fracture-controlled flow zones identified from hydrogeological logging (Milodowski et al., 1997, 2002; Gutmanis et al., 1998) (e.g. Fig. 2). Several of the permeable sandstone intervals identified in the upper part of the Sherwood Sandstone Group are also closely associated with staining by ME8 iron and manganese oxyhydroxides. Gutmanis et al. (1998) considered that the presence of ME8 and ME9 mineralisation was the best indicator of potential hydraulically active fractures (i.e. potentially flowing features – PFFs) in the deep boreholes. The distribution of these PFFs in the BVG is partially correlated with fault zones: clusters of PFFs are often associated with fracture damage zones in the footwall or hanging-wall of faults.

4.3. Morphology and crystal growth zoning in ME9 calcite

The morphology of ME9 calcite crystals appears to vary systematically with groundwater salinity in all the deep boreholes (Figs. 3 and 4). Calcite in the shallow fresh groundwater zone is characterised by

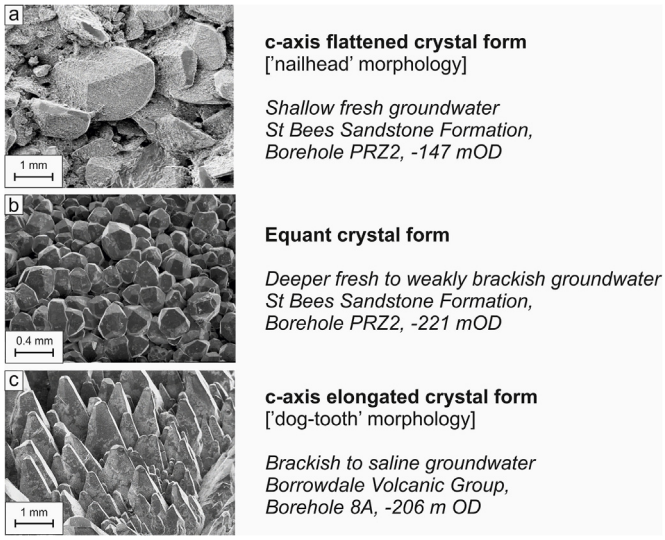

Fig. 3. SEM images illustrating the different morphological characteristics of ME9 calcite: [a] c-axis flattened or 'nailhead' crystal form characteristic of the shallow fresh groundwater; [b] equant crystal form characteristic of the deeper freshwater to weakly brackish groundwater; [c] c-axis elongated or 'dog-tooth crystal form characteristic of deeper saline groundwater.

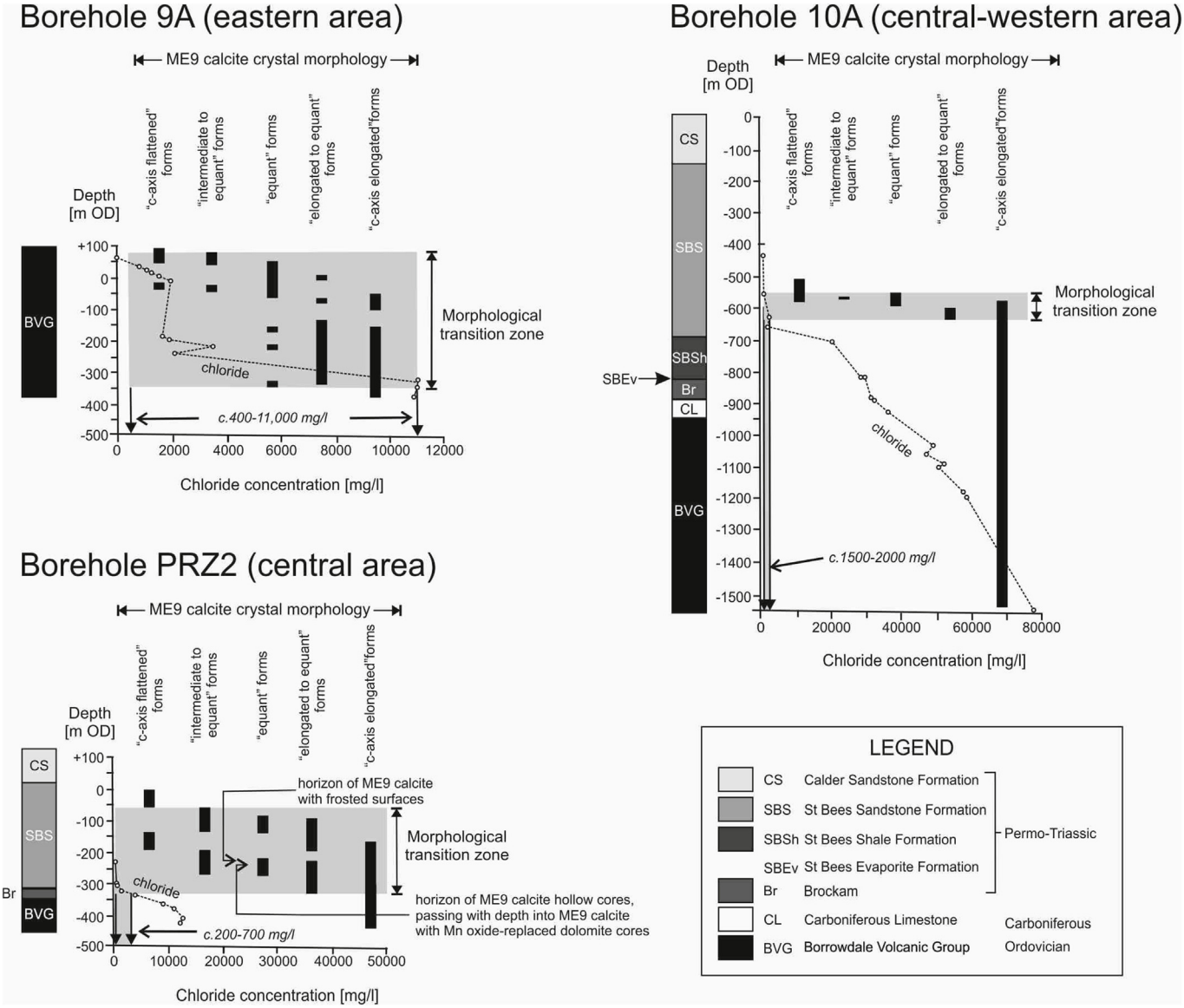

Fig. 4. Distribution of ME9 calcite crystal morphological types, and comparison with variations in present-day groundwater salinity (chloride concentration) for boreholes 9, 10A and PRZ2.

squat or c-axis shortened ('nailhead') crystal forms (Fig. 3a). Crystals become more equant (Fig. 3b) as the salinity increases towards the base of the fresh groundwater zone and becomes weakly saline or brackish, and progressively changes to c-axis elongated ('dog-tooth') crystal forms (Fig. 3c) as salinity increases into the saline groundwater zone. The crystal shape is unrelated to the grain size, and the same morphological variation is observed at all scales ranging from a few microns to crystals several millimetres in size. The morphological variation is independent of lithostratigraphy and absolute depth but closely mirrors the topology of the transition from fresh groundwater to saline groundwater, which occurs at different depths and lithologies in different boreholes across the area (e.g. Fig. 4). The depth interval over which the change in morphology (Morphological Transition Zone, MTZ) between c-axis elongated to short c-axis occurs varies markedly across the study area (Fig. 4). In the east, the top of the MTZ starts at a shallow depth of approximately 50 m below ground level (−7 m OD) but occurs over a very wide (390 m wide) interval (e.g. borehole 9A). There is considerable overlap in the ranges of the different morphological types in this part of the area, with the MTZ spanning the range in the salinity from 400 to 11,000 mg/L chloride of the present-day groundwaters. The MTZ deepens and becomes narrower westward: in the central area, its top is at a depth of about 165 m depth (approximately −55 m OD) and is approximately 270 m wide (e.g. borehole PRZ2), corresponding to a much narrower range in salinity from 200 to 700 mg/L chloride; and in borehole 10A (which lies in the Fleming Hall Fault Zone) the MTZ is still narrower, starting at about 600 m depth (approximately −550 m OD) and only about 80 m wide (Fig. 4).

Cathodoluminescence petrography reveals a marked difference in the luminescence and growth zoning characteristics between ME9 calcite from the shallow fresh groundwater zone and ME9 calcite in the deeper brackish to saline groundwater zone (Fig. 5). Calcite from above the MTZ, in the upper part of freshwater zone, is characterised by sharply-defined concentric growth zones comprising strongly-contrasting alternating yellow-to-orange, very brightly-luminescent and non-luminescent bands (e.g. Fig. 5a). In several cases, the growth zones are dominated by non-luminescent calcite with very fine bright-luminescent bands often only a few microns wide. CL observations often show that the calcite has nucleated upon corroded relicts of earlier (usually Mesozoic ME6c - cf. Table 2) calcite mineralisation. No correlation of the growth zoning stratigraphy could be made between

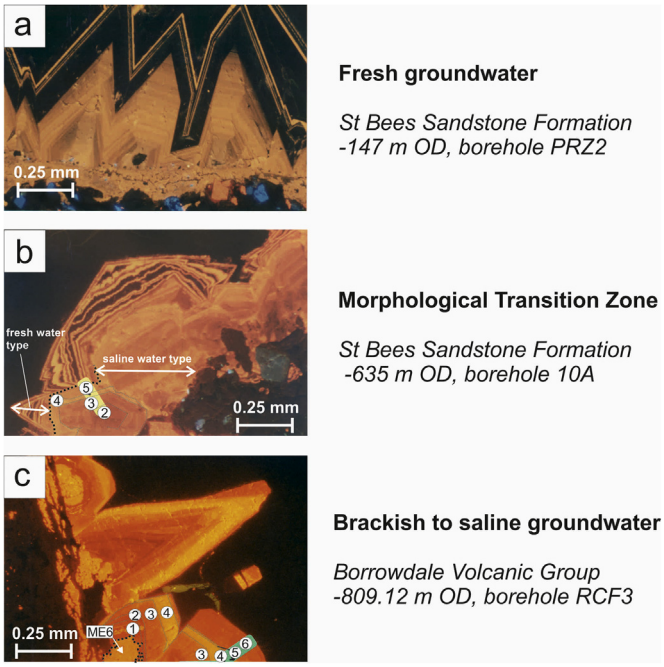

Fig. 5. CL images illustrating the growth zoning characteristic of ME9 calcite: [a] strongly-zoned bright- and non-luminescent growth zones in ME9 calcite from shallow fresh groundwater; [b] ME9 calcite from the morphological transition zone (MTZ) in the deeper freshwater to weakly brackish groundwater, showing syntaxial overgrowth 'freshwater-type' calcite earlier 'saline groundwater-type' calcite, accompanied by change in crystal growth morphology; [c] zoned moderately bright- and dull-luminescent growth zones in ME9 calcite from deep saline groundwater, nucleated around corroded cores of ME6 calcite. Growth zones are numbered as described in the text.

different fractures. In some cases, the ME9 calcite contains inclusions of very fine grained opaque black or dark brown manganese or mixed manganese-iron oxyhydroxide.

Calcites within the saline groundwater zone and below the MTZ typically also display well-developed concentric growth zoning. However, in this case the growth zones consist of moderately-to-brightly, yellow-luminescent oscillating with intermediate orange-luminescent and dull dark orange to reddish luminescence bands (e.g. Fig. 5c). Faint, micron-scale concentric zones of varying luminescence can also be discriminated within the coarser luminescent zones but on the whole, the growth-zoning is not as fine-scaled as that seen in the 'above MTZ' calcite. CL reveals that ME9 calcite usually contains corroded relict cores of old (ME6c) calcite, around which the ME9 calcite has nucleated as a syntaxial overgrowth (Fig. 5c). Minor to trace amounts of pyrite and marcasite may encrust the ME9 calcite and line some fractures associated with ME9 mineralisation in the BVG basement rocks. Trace amounts of these iron sulphides are also sometimes seen as very fine-grained inclusions within the brighter-luminescent zones, typically concentrated as a thin film or as a fine 'dusting' on the preceding duller-luminescent calcite substrate or coating the corroded surfaces of ME6c calcite cores.

Up to eight coarse but distinct CL zones (referred to here as Zones 1 (oldest) to 8 (youngest)) can be distinguished in ME9 calcite within the saline groundwater zone below the MTZ. The calcite substrate beneath successive zones may be etched and corroded. The growth zone 'stratigraphy' can be correlated between calcites from different fractures over substantial depth intervals within the same borehole, and between different boreholes across the area. However, the differentiation between Zones 2 and 3, and Zones 5 and 6, is often indistinct and gradational. The development of the CL zoning pattern also varies systematically from east to west across the study area: the most complete zoning stratigraphy (Zones 1 to 8) is found in ME9 calcite from boreholes in the east (boreholes 8A, 8B and 9); in boreholes in the central part of the area the calcite typically displays Zones 1 to 6 or 1 to 7; further west (boreholes 10A and 12A) only Zones 1 to 4 may be developed, reducing to only Zones 1 to 3 at depth.

ME9 calcite within the upper part of the MTZ displays similar CL characteristics to 'above MTZ' calcite higher up in the freshwater zone. However, deeper into and towards the base of the MTZ the ME9 calcite displays a more complex growth history and zonation pattern. It comprises overgrowths of calcite, with CL characteristic of the freshwater zone calcite found above the MTZ that has nucleated on top of 'below MTZ' calcite (Fig. 5b). The interface between these two types of calcite is often corroded. CL observations also show that change from 'below MTZ' calcite to 'above MTZ' calcite is accompanied by a change in the preferential growth direction of the crystal faces (Fig. 5b), which is reflected in the overall change in crystal morphology observed in passing from saline to freshwater. This implies that within the MTZ, the groundwater from which the ME9 calcite has precipitated has evolved from saline to freshwater, during the period that the calcite crystals grew. The reverse trend, of saline groundwater-type calcite growing on top of freshwater-type calcite is not observed in any of the ME9 mineralisation.

4.4. Chemical composition (Fe, Mn, REEs) of ME9 calcite

Luminescence in calcites is predominantly controlled by variation of Mn and Fe contents (Marshall, 1988; Myers, 1991; Machel and Burton, 1991; Savard et al., 1995). Degrees of luminescence of individual CL zones in ME9 calcite (Fig. 5) have therefore been interpreted to be indicative of variations of Mn and Fe contents (Milodowski et al., 1998, 2005; Bath et al., 2000). Concentrations of Mn and Fe in groundwaters are sensitive to redox, amongst other variables including complexation in groundwaters with higher salinities, so Mn and Fe contents of secondary calcite inferred from luminescence have been interpreted to reflect redox conditions in the groundwaters from which the calcites (or calcite growth zones) precipitated (Barnaby and Rimstidt, 1989). Analyses by EMPA of Mg, Mn, Fe, Sr and Ba in growth zones, identified by their varying luminescence, of seven representative samples of ME9 calcite are given in Supplementary Table S3. Fig. 6 illustrates compositional data and the corresponding Cl patterns for two samples representative of freshwater and saline groundwater type calcite, respectively.

In the freshwater ('above MTZ) calcite, the non-luminescent growth zones are non-ferroan non-manganoan calcite, whereas the brightly luminescent calcite zones contain significant Mn^{2+} (300-12,000 ppm) but Fe^{2+} is very low or absent (typically < 250 ppm) (Fig. 6a). Studies have shown only as little as 20 ppm Mn^{2+} is required to activate luminescence, whereas luminescence is partially quenched at Fe^{2+} concentrations in excess of 1400 ppm (Savard et al., 1995).

The saline groundwater ('below MTZ') calcites display a different relationship between luminescence, and Mn^{2+} and Fe^{2+} concentration (Fig. 6b). These calcites are all significantly ferro-manganoan but the luminescence broadly reflects variations in the Mn: Fe ratio: brighter luminescence generally corresponds to higher Mn: Fe; whereas, duller luminescence generally corresponds to lower Mn: Fe. Although often brightly luminescent, the relict cores of ME6 calcite within the ME9 calcite sometimes show abnormally high Fe concentrations. This is probably due to the presence of fine grained hematite inclusions, which are often intimately associated with the ME6 mineralisation.

LA-ICPMS analyses also show a covariance between Fe and Mn (Fig. 7). Mn and Fe are both relatively low in the calcites from above the fresh-saline transition, and Mn varies more than Fe. In contrast, ME9 calcites from below the MTZ in the saline groundwater zone are much more ferromanganoan with up to an order of magnitude more Mn and Fe. However, there is no systematic variation of Mn and Fe with depth in calcites below the MTZ (Fig. 7), and the total Fe and Mn content may be locally controlled. Higher Fe and Mn contents of calcite

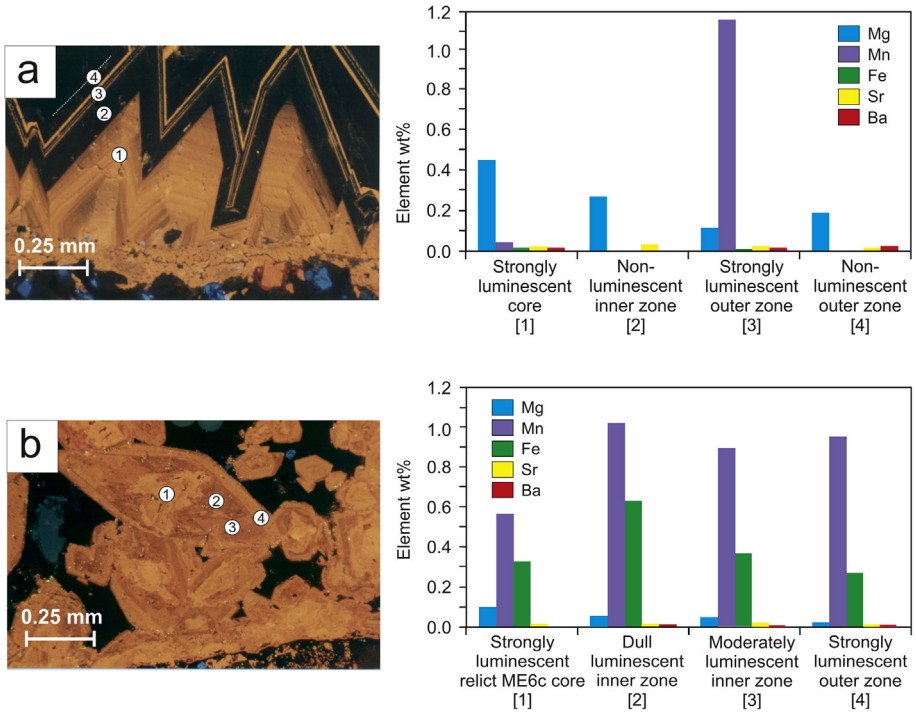

Fig. 6. EMPA analyses of minor and trace elements (Fe, Mn, Mg, Sr and Ba) in ME9 calcite growth zones: [a] non-luminescent and brightly luminescent growth zones in typical 'above MTZ' calcite, from the freshwater zone in the St Bees Sandstone Formation aquifer, borehole PRZ2, -147 m OD; [b] dull-luminescent and bright-luminescent CL growth zones in typical 'below MTZ' calcite from the saline groundwater zone in the BVG, borehole PRZ2, -407 m OD.

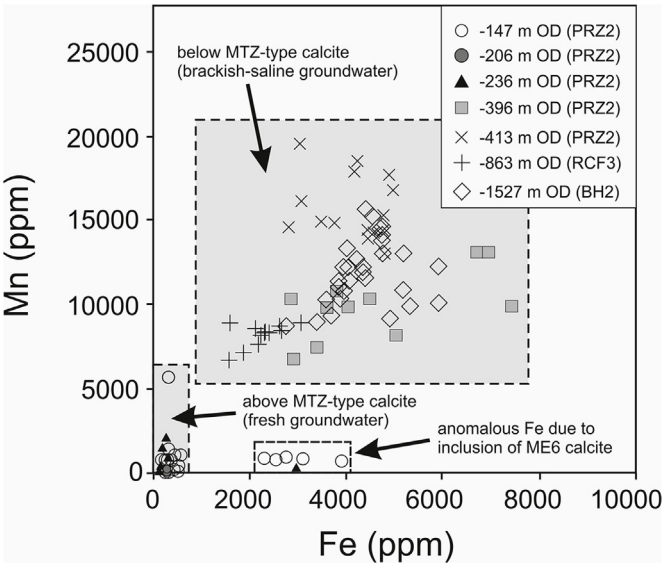

Fig. 7. Variation in Mn and Fe concentrations determined by LA-ICPMS in ME9 calcites from different depths from boreholes in the central area.

below the MTZ also correspond to higher Fe^{2+} and Mn^{2+} in saline and brine groundwaters which is attributed to complexation (Table 1). Therefore, the contents of Fe and Mn in secondary calcites are controlled both by redox and groundwater salinity at the time of precipitation.

A small amount of Mg is present in the ME9 calcite (Fig. 6 and Supplementary Table S3). Calcites from above the MTZ in the freshwater zone (200–4500 ppm) contain slightly more Mg than calcites below the MTZ (< 600 ppm). The incorporation of magnesium has been considered a principal factor influencing calcite morphology in previous studies of both natural and experimental systems (Folk, 1974; Lahann, 1978; Davis et al., 2015). These studies suggested Mg affects calcite crystal growth kinetics by inhibiting nucleation on certain crystal faces, thereby reducing accretion in the c-axis crystallographic through: (i) lattice distortion and contraction; (ii) influencing surface charge and complexation phenomena, thereby affecting growth kinetics. Magnesium concentration increases with depth and salinity in the groundwaters from west Cumbria (Table 1), and the observed morphological change in from c-axis flattened to c-axis elongated crystal forms is consistent with this. However, the slightly higher concentration of Mg within ME9 calcite above the MTZ appears to be contradict this. Therefore, other factors such as other chemical components (e.g. organics, SO_4, Mn^{2+} Sr^{2+} (Parker et al., 1993; Kimbell and Humphrey, 1994; Temman et al., 2000; Astilleros et al., 2002)), degree of saturation, warmer temperature or higher fluid flow rates (Given and Wilkinson, 1985; Gonzalez et al., 1992) may also have influenced the calcite morphology. The precise control on the calcite growth morphology remains unexplained.

Ce is the only one of the REEs that can exist in either the trivalent or tetravalent oxidation states within the normal range of shallow, low-temperature groundwater conditions. Therefore, variations in Ce concentrations in relation to the other REEs are a potential indicator of redox. Ce^{4+} is considerably less mobile than Ce^{3+}, and Ce anomalies in sedimentary and diagenetic carbonates have been recognised as sensitive indicators of variations in oxic conditions in near-surface chemical systems (Humphris, 1984; McLennan, 1989; Braun et al., 1990; Leybourne et al., 2000).

ΣREE (total of REE concentrations) in ME9 calcite varies between about 1 and 2 ppm and 350 ppm but does not vary systematically with depth. Chondrite-normalised REE data for ME9 calcites from below the MTZ and in the saline groundwater zone are characterised by a "flat" or slight "hump-like" distribution pattern, associated with a relative enrichment of middle rare earth elements (MREE), compared to light rare earth elements (LREE) or heavy rare earth elements (HREE) (as shown in the example in Fig. 8a). There is no systematic variation in REE distribution pattern or abundance between dull-luminescent and brightly-luminescent growth zones in these saline groundwater zone calcites. Ce shows no anomalous behaviour and therefore appears to have behaved geochemically the same as the other trivalent REEs, remaining in the reduced form Ce^{3+}.

In contrast, ME9 calcite from above the MTZ shows a marked difference in the REE chemistry between the non-luminescent and brightly luminescent growth zones (as shown by the example in Fig. 8b and c).

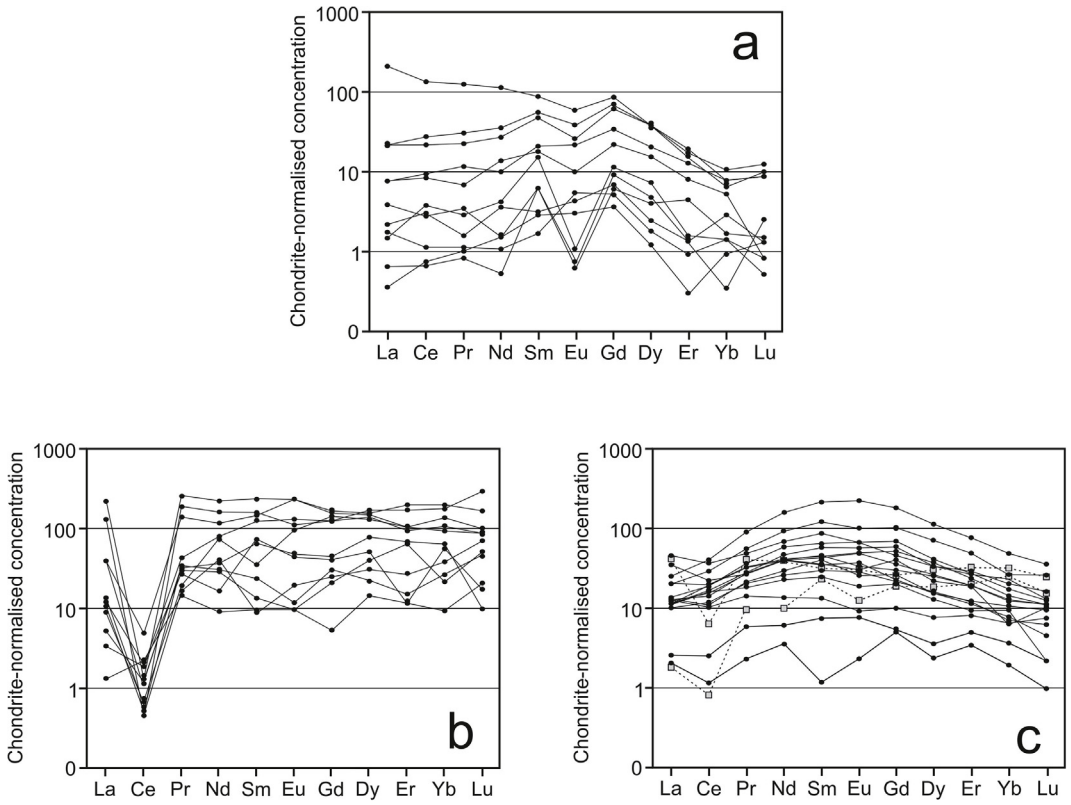

Fig. 8. Chondrite-normalised REE distribution patterns determined by LA-ICPMS for growth-zones in ME9 calcite. [a] Dull-luminescent and bright-luminescent CL growth zones in typical 'below MTZ' calcite from the saline groundwater zone in the BVG, borehole, −1527 m OD. [b] Non-luminescent CL growth zones and [c] brightly-luminescent CL growth zones, in a typical 'above MTZ' calcite from the freshwater zone in the St Bees Sandstone Formation aquifer, borehole PRZ2, -147 m OD.

Chondrite-normalised REE patterns for the non-manganoan, non-ferroan non-luminescent calcite show that cerium (Ce) is very strongly depleted by up to three orders of magnitude relative to the other REEs. In contrast, the brightly-luminescent manganese-rich non-ferroan calcite zones have no negative Ce anomaly. This shows that Ce behaved very differently to the other trivalent REEs during the growth of the non-luminescent calcite but behaved similarly to the other REEs when the brightly luminescent calcite was precipitating.

Observations on the ME9 calcites from above the MTZ therefore imply that the groundwater conditions were more oxidising during the growth of the non-luminescent calcite, with Ce in the groundwater present at lower concentrations as the less soluble Ce^{4+}. However, during the growth of the brightly-luminescent calcite, Ce shows similar behaviour to the other REEs and therefore indicates that the groundwater was more reducing with a higher concentration of Ce present in the more soluble Ce^{3+} state. Chondrite-normalised REE patterns for the brightly-luminescent manganoan calcite above the MTZ (Fig. 8c) are very similar to that observed in ferromanganoan ME9 calcite from below the MTZ (Fig. 8a).

ME9 calcite showing anomalous Ce behaviour is only observed in the 'above-MTZ' calcite in the freshwater zone, and in overgrowths of this calcite that have nucleated on 'below-MTZ' calcite within the MTZ. No evidence of calcite showing anomalous Ce behaviour was found in ME9 calcite below the MTZ. Detailed observations from boreholes in the centre of the study area show that 'above-MTZ' calcites with anomalous negative Ce are restricted to the upper part of the Sherwood

Table 3
Summary showing correspondence of ME9 calcites with negative cerium anomalies, with growth zone luminescence characteristics and depth, in boreholes from the centre of the study area.

Borehole	Depth (m OD)	Lithology	Above MTZ calcite growth zone CL characeristics		Below MTZ calcite growth zone CL characeristics	
			Non Lum.	Bright Lum.	Bright Lum.	Dull Lum.
PRZ2	−147	St Bees Sandstone	−ve Ce anomaly	No Ce anomaly	Below MTZ type calcite absent	
PRZ2	−206	St Bees Sandstone	−ve Ce anomaly	No Ce anomaly	Below MTZ type calcite absent	
PRZ2	−221	St Bees Sandstone	No Ce data		Below MTZ type calcite absent	
PRZ2	−236	St Bees Sandstone	−ve Ce anomaly	No Ce anomaly	Below MTZ type calcite absent	
PRZ2	−243	St Bees Sandstone	No Ce data		Below MTZ type calcite absent	
PRZ2	−278	St Bees Sandstone	Above MTZ type calcite absent		No Ce anomaly	No Ce anomaly
RCF1	−399	Brockram	Above MTZ type calcite absent		No Ce anomaly	No Ce anomaly
PRZ3	−396	BVG	Above MTZ type calcite absent		No Ce anomaly	No Ce anomaly
PRZ2	−413	BVG	Above MTZ type calcite absent		No Ce anomaly	No Ce anomaly
RCF1	−548	BVG	Above MTZ type calcite absent		No Ce anomaly	No Ce anomaly
RCF1	−837	BVG	Above MTZ type calcite absent		No Ce anomaly	No Ce anomaly
BH2	−1527	BVG	Above MTZ type calcite absent		No Ce anomaly	No Ce anomaly

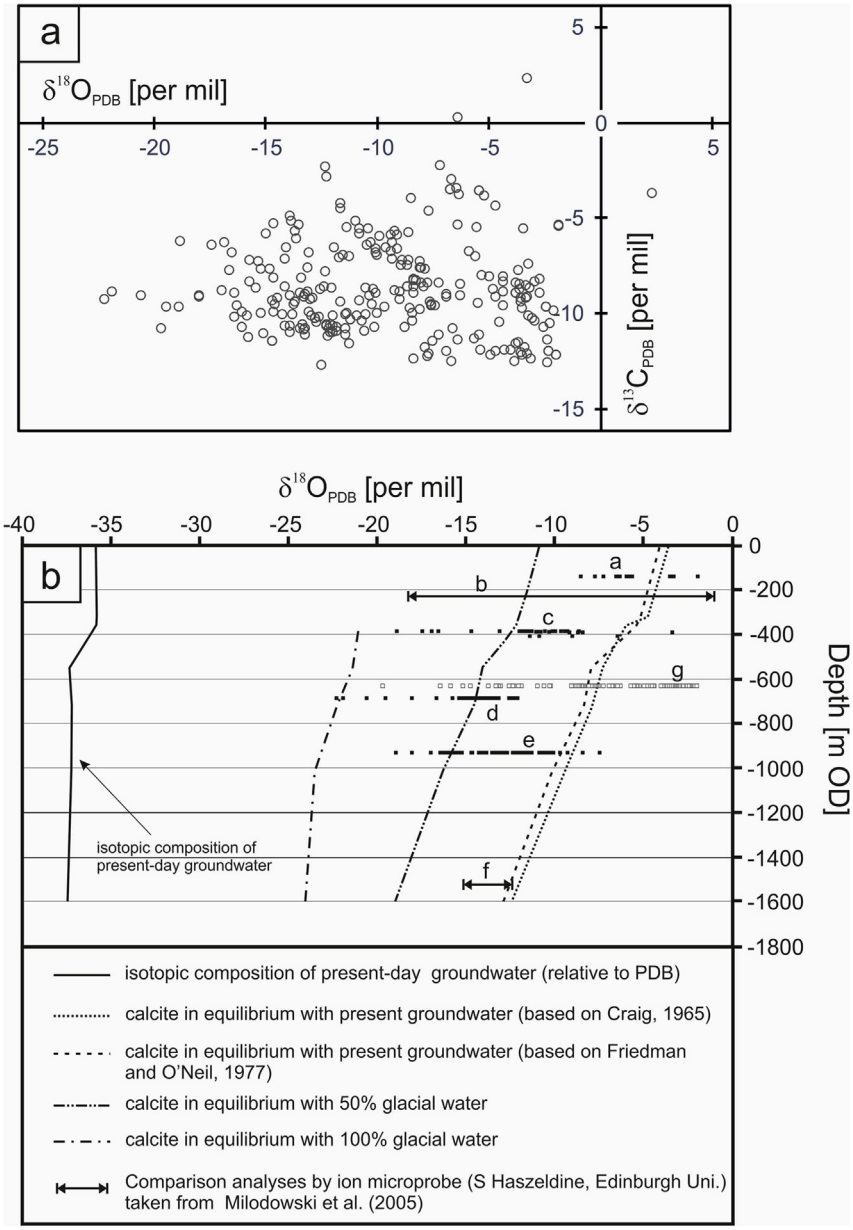

Fig. 9. Ranges of oxygen isotope composition for individual ME9 calcites from different depths, micro-sampled across crystal growth zones by He-LACE and diamond micro-drilling. Samples include: (a) PRZ2 -147 m OD; (b) PRZ2 -206 m OD; (c) PRZ2 -413 m OD, PRZ2 -396 m OD, RCF1 -390 m OD; (d) RCF1 -690 m OD; (e) RCF1 -938 m OD; (f) borehole 2 −1528 m OD; (g) borehole 10A −635 m OD. Modelled calcite composition curves are shown for calcite precipitated in equilibrium with: (i) present-day groundwater (based on equations of Craig, 1965 or Friedman and O'Neil, 1977), (ii) 50% glacial water component; (iii) 100% glacial water component. Curves for (ii) and (iii) have been calculated using equation of Friedman and O'Neil, 1977). Glacial meltwater assumed to have $\delta^{18}O$ of −20‰$_{SMOW}$). Data obtained by ion microprobe (S. Haszeldine, Edinburgh University) from two ME9 calcites are shown for comparison (taken from Milodowski et al., 2005).

Sandstone Group aquifer, above about −250 m OD (Table 3). No evidence of anomalous Ce behaviour is displayed in calcite from the deeper parts of sedimentary cover rocks below this depth, nor in the BVG basement (Table 3). Strongly-zoned 'above-MTZ' calcite does occur to greater depth in the sandstone aquifer further west, in boreholes 10A (−636 m OD) and 12A (−534 m OD) but was not found below this depth in either the Permo-Triassic and Carboniferous sedimentary strata or basement lithologies.

4.5. Stable ($\delta^{13}C$ and $\delta^{18}O$) isotope composition of ME9 calcite

Stable ($\delta^{13}C$ and $\delta^{18}O$) isotope data obtained by He-LACE from the small number of ME9 calcites are provided in Supplementary Table S4. ME9 calcite shows a wide variation in $\delta^{18}O$ from about −22 to −2 ‰$_{PDB}$, whereas $\delta^{13}C$ has a much more limited variation between −2 and −12 ‰$_{PDB}$ (Fig. 9a). In contrast to fracture calcites from deep groundwater systems in the Fennoscandinavian Shield (Drake and Tullborg, 2009; Drake et al., 2015), no extremely light or heavy $\delta^{13}C$ values indicative of microbial methane oxidation or deep methanogenesis were observed. The ME9 calcite $\delta^{13}C$ values are best explained by either: (i) precipitation associated with bacterial reduction of iron, manganese and sulphate (e.g. Mozley and Burns, 1993), or alternatively; (ii) from groundwater dominated by bicarbonate derived through the dissolution of older ME6 carbonate minerals, which have similar $\delta^{13}C$ (Milodowski et al., 1998) and are observed to be dissolving up-gradient in the shallow Permo-Triassic, and in the BVG in the recharge area to the east.

Fig. 9b illustrates the range in $\delta^{18}O$ values ME9 calcite from different depths. Calcites from the Permo-Triassic sedimentary cover rocks (Fig. 9b: samples a-c and g) display the greatest range in $\delta^{18}O$ (−19 to −2 ‰$_{PDB}$). Deeper samples from the BVG have $\delta^{18}O$ values between −23 and −7 ‰$_{PDB}$; the most negative values exhibited by the calcite sample from −690 m OD in borehole RCF1, but overall becoming less depleted in ^{18}O with increasing depth (Fig. 9b: samples d-f). The $\delta^{18}O$ values obtained by ion microprobe (cf. Milodowski et al., 2005) are also plotted for comparison in Fig. 9b. The deepest ME9 calcite studied (-1527 m OD in borehole 2) exhibited only a relatively narrow range in isotopic composition (−16 to −13 ‰$_{PDB}$ $\delta^{18}O$) compared to the shallower ME9 calcites from the same area. Reconciling the He-LACE analyses points precisely with the calcite growth zones differentiated by

CL microscopy was very difficult because the zones were often too fine to be resolved during analysis. Furthermore, the poor surface finish of sample mounts prepared in gypsum plaster for He-LACE was not conducive to CL imaging. However, samples subsequently mounted in M70 alloy did enable the $\delta^{13}C$ and $\delta^{18}O$ analyses to be correlated specific CL zones in the ME9 calcites (see Supplementary Table S4). Where this correlation was possible, the cores of the ME9 calcite were found to be isotopically very light and depleted in $\delta^{18}O$, whereas the outermost part of the ME9 calcite crystals have heavier $\delta^{18}O$ that is consistent with the calculated isotopic composition (Craig, 1965; Friedman and O'Neil, 1977) of calcite in equilibrium with the present groundwaters (shown in Fig. 9a). Calcite analyses with heavier $\delta^{18}O$ values appear to correspond to fragments of old ME6c calcite upon which the ME9 calcite overgrowths have been seeded.

4.6. Strontium isotope ratios of ME9 calcite

Strontium isotope ($^{87}Sr/^{86}Sr$) ratios for ME9 calcite (Supplementary Table S5) can be compared with the $^{87}Sr/^{86}Sr$ ratios of present-day groundwater from the boreholes (Table 1). The $^{87}Sr/^{86}Sr$ ratio in the calcites varies with depth and laterally across the area. However, their values fall within the range of the groundwater $^{87}Sr/^{86}Sr$ ratios. The data represent 'whole crystal' analyses and therefore do not take into account variation within individual growth zones or presence of included relicts of earlier carbonate mineralisation. Nevertheless, the $^{87}Sr/^{86}Sr$ ratios of the calcite are still consistent with precipitation from the present groundwaters.

4.7. Fluid inclusions in ME9 calcite

In general, fluid inclusions are only very sparsely distributed within the ME9 calcites. Furthermore, the majority of fluid inclusions are preserved only within the central region of the crystals and in particular, they tend to be concentrated along the boundary between corroded relict cores of older (ME6) calcite and the enclosing ME9 calcite. The outer, more recent, calcite growth zones contained very few, if any, fluid inclusions suitable for analysis. Consequently, most of the fluid inclusion data probably represent the earliest stage of ME9 mineralisation, whilst the later growth zones are poorly or unrepresented.

The microthermometric measurements for fluid inclusions in ME9 calcite are presented in Supplementary Table S6. The fluid inclusions in ME9 calcites are all monophase inclusions, which indicates they formed below 80 °C (Roedder, 1984). This is quite distinct from the two-phase liquid-vapour inclusions that characterise inclusions found in older ME6 and ME2 calcite mineralisation (Milodowski et al., 1998).

Salinity estimates from T_{ice} for most inclusions are between 3000 and 50,000 mg/L TDS. The detection limit for fluid inclusion salinity determination is limited by the precision of the temperature measurement, which is ± 0.1 °C. This equates to a precision of 0.2 wt% NaCl (i.e. 2000 mg/L NaCl). This means it is difficult to reliably differentiate more dilute brackish waters from freshwater in these calcite samples. Higher salinities (up to 213,000 mg/L TDS) were recorded in many of the calcites from boreholes 11A, 12A (Supplementary Table S6), which are located in the south-west of the area and closer to the coast (Fig. 1). In general, fluid inclusion salinity increases with depth with higher values found in BVG and Brockram than in the overlying sandstones of the Sherwood Sandstone Group. However, some calcite samples display a wide variation in fluid inclusion salinity. The lower salinity fluids have T_{fm} and T_{ice} values that are characteristic of an alkali-bicarbonate fluid composition, whereas the higher salinity inclusions have T_{fm} values that are consistent with a Na-Cl fluid composition.

The fluid inclusion salinities are similar to the range of salinity found in groundwaters in the study area at the present-day (~200–188,000 mg/L TDS). However, a significant proportion of the ME9 calcite fluid inclusions have salinities that are substantially higher than those of present-day groundwater at the same depth: for example, in the centre of the study area where the salinity of present-day groundwaters reaches about 25,000 mg/L TDS, whereas some fluid inclusions in ME9 calcite analysed from boreholes RCF1, RCF2, RCF3 and PRZ2 have salinities exceeding 50,000 mg/L. This clearly indicates that groundwaters were more saline during the formation of the part of these calcites from which the inclusions are preserved.

LA-ICPMS microchemical analyses of fluid inclusions from ME9 calcites are presented in (Supplementary Table S7). Analytical detection limits meant that only the brackish and more saline inclusions could be analysed. More dilute and freshwater inclusions were at or below detection. Fig. 10 compares the microchemical analyses of fluid inclusions in ME9 calcite from boreholes 10A, RCF1 and PRZ2 with present-day deep groundwaters. This shows that the fluid inclusion compositions lie close to a mixing line between the average composition of basinal brines and basement saline groundwaters (Bath et al., 2006).

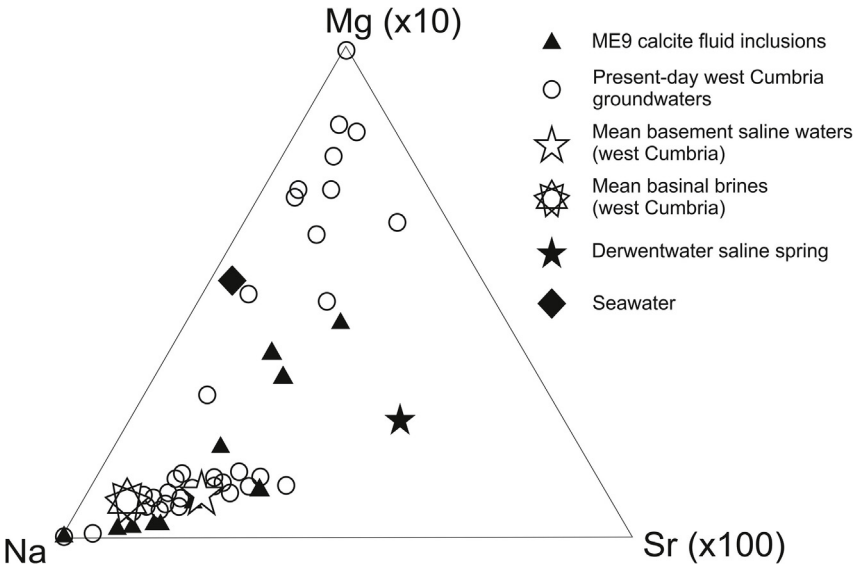

Fig. 10. Comparison of Na:Mg:Sr ratios for saline fluid inclusions analysed by LA-ICPMS with present-day west Cumbrian groundwaters in the Nirex boreholes and saline springs from the Lake District.

Table 4
Summary of radiometric ages determined for secondary ME8 and ME9 fracture minerals.

Mineral	Sample No	Nirex borehole	Depth (m OD)	Host rock	Age	Dating method
ME8 Mn oxyhydroxide	NSF2/1307/P4	2	60[a]	Calder Sst	26.39 Ma	^{40}Ar–^{39}Ar total gas age
ME8 Mn oxyhydroxide	NSF2/1307/P4	2	60[a]	Calder Sst	14 – 21 Ma	^{40}Ar–^{39}Ar plateau age
ME8 Mn oxyhydroxide	PRZ2/5/P4	PRZ2	−321[a]	St Bees Sst	276 Ma[a]	^{40}Ar–^{39}Ar total gas age[b]
ME9 calcite [whole crystal]	RCF1/86/P4	RCF1	−536	BVG	74 ka (+48/−33)	$^{230}Th/^{234}U$ HRICPMS pseudo-isochron pure and impure calcite
ME9 calcite [whole crystal]	B947 [NSF2/1321/P4]	2	−878	BVG	105 ka (+104 /−55)	$^{230}Th/^{234}U$ HRICPMS pseudo-isochron
ME9 calcite [whole crystal]	C848 [NSF5/672/P4]	5	−295	St Bees Sst	267 ka (+32/−24)	$^{230}Th/^{234}U$ HRICPMS total dissolution
ME9 calcite [whole crystal]	C848 [NSF5/672/P4]	5	−295	St Bees Sst	300 ka (+45/−33)	$^{230}Th/^{234}U$ HRICPMS total dissolution [duplicate]
ME9 calcite [whole crystal]	C848 [NSF5/672/P4]	5	−295	St Bees Sst	245 ka (+26/−21)	$^{230}Th/^{234}U$ HRICPMS calcite leachate
ME9 calcite [whole crystal]	C848 [NSF5/672/P4]	5	−295	St Bees Sst	289 ka (+25/−22)	$^{230}Th/^{234}U$ HRICPMS calcite leachate [duplicate]
ME9 calcite [whole crystal]	PRZ2/16/P4	PRZ2	−274	St Bees Sst	70 ka (+300/−70)	$^{230}Th/^{234}U$ HRICPMS pseudo-isochron pure calcite
ME9 calcite [whole crystal]	B946 [NSF2/1301/P4]	2	−1527	BVG	21 ka (± 9)	$^{230}Th/^{234}U$ Alpha spectrometry
ME9 calcite [whole crystal]	C440 [RCF3/303/P4]	RCF3	−901	BVG	> 300 ka	$^{230}Th/^{234}U$ HRICPMS calcite leachate
ME9 calcite [whole crystal]	NFS10A/1/P4	10A	−633	St Bees Sst	17 − 65 ka	$^{230}Th/^{234}U$ TIMS corrected for ^{230}Th from wallrock and hematite impurities
ME9 calcite Individual crystal core growth zone only	D750	10A	−635	St Bees Sst	(a) 6.44 (± 0.28) Ma (b) 6.36 (± 0.43) Ma	U-Pb LA-PIMMS[b]

Notes:
[a] Depth by reference to depth below drilling rotary table rather than depth below OD.
[b] Age unreliable – total gas age dominated by argon contributed from unresolved illite contamination.
Data from Nirex (1998a) except for LA-PIMMS data** for sample D750 provided courtesy Dr N Roberts (pers. comm.).

4.8. Timing of ME8 and ME9 mineralisation

Radiometric ages were previously obtained for 2 samples of ME8 manganese oxyhydroxide and 10 samples ME9 calcite mineralisation as part of the regional fault dating study (Nirex, 1998a) and are presented in Table 4.

The ME8 sample from a depth of 60 m in borehole 2 gave an ^{40}Ar-^{39}Ar 'total gas age' of between 26 and 39 Ma and a slightly younger ^{40}Ar-^{39}Ar 'plateau age' of 14–21 Ma. The ^{40}Ar-^{39}Ar 'total gas age' of the ME8 manganese oxyhydroxide mineralisation from borehole PRZ2 is unrealistic as it is dominated by Ar from significant illite contamination derived from the sandstone wallrock. These limited age data indicate that ME8 mineralisation may extend at least as far back as the Miocene. However, the presence of similar mineralisation cementing Pleistocene fluvioglacial deposits (penetrating into the underlying bedrock) and associated with some groundwater seeps in the Sherwood Sandstone at outcrop, indicates that this alteration is ongoing (Milodowski et al., 1998). ME8 is attributed to supergene (near-surface) weathering and oxidation that was probably initiated following regional uplift during Miocene (Chadwick et al., 1993, 1994; Holliday, 1993) and is continuing to the present day in the near-surface oxidising fresh groundwater zone.

Dating the ME9 calcite by the $^{230}Th/^{234}U$ method proved difficult due to very low uranium concentrations: shown by LA-ICPMS to be typically < 0.1 ppm U in most cases. This was compounded by the small amounts of sample available, and the presence of traces of hematite and clay which could potentially contribute some uranium and thorium. Consequently, the ages for ME9 shown in Table 4 have relatively large uncertainties. The 10 ME9 calcites analysed yielded ages ranging from 17 to 300 ka. Replicate ages obtained by different methods for one sample from the St Bees Sandstone Formation at a depth of −295 m OD in borehole 5, gave reasonably reproducible ages of between 245 and 300 ka. However, because the ME9 calcites are strongly-zoned, these 'whole crystal' ages must represent "mixed" or average ages: the early growth zones will be older and outer growth zones may be relatively recent although, the analyses are biased

towards younger ME9 growth zones since material was sampled predominantly from the outer parts of the calcite crystals. This means that the data cannot be correlated with specific Quaternary events. Nevertheless, the results still indicate that at least part of the ME9 calcite mineralisation is Quaternary in age, with the caveat that the early stages of ME9 calcite growth may be significantly older. Attempts have subsequently been made to obtain U-Pb ages resolved from individual growth zones in same calcites by using the recently-developed high-resolution laser ablation – plasma ionisation multi-collector mass spectrometry (LA-PIMMS) method described by Roberts and Walker (2016). Seven samples of hand-picked pure ME9 calcite crystals were submitted for analysis. Unfortunately, the U contents of most growth zones in the ME9 calcite were far too low (shown by LA-ICPMS to be typically < 0.1 ppm, and often below detection) to determine the age reliably, except for the core zone of ME9 calcite from one sample (sample D750 from borehole 10A, Table 4). This gave a late Miocene age of 6.4 Ma for the innermost zone of ME9 calcite (based on 17 analysis points) in this sample (N. Roberts, personal communication). This may indicate that like ME8 at shallow depths, ME9 calcite formation may have been ongoing at least since Miocene uplift.

5. Palaeohydrogeological interpretation of data from groundwaters and secondary minerals

5.1. Groundwater sources and movements

Fresh-brackish groundwaters from sedimentary cover rocks of the coastal plain and outcropping basement rocks in the eastern part of the study area mostly have stable isotopic compositions similar to present-day recharge (−6.8 to −6‰ $\delta^{18}O$; Table 1). Saline groundwaters in basement rocks and in deeper sedimentary cover rocks in the centre and western parts of the study area have lighter isotopic compositions (−8 to −7‰ $\delta^{18}O$). The transition and mixing zone between brackish and saline groundwaters with distinctive isotopic compositions occupies a fairly narrow depth interval in the inland part of the study area (Bath et al., 1996, 2006). Below that, saline groundwaters with lighter isotopic compositions are found to more than 1000 m depth in basement rocks. The stable isotope compositions indicate that the water originated in a colder climate than at present.

Isotopically-light water is interpreted as having infiltrated during the Pleistocene glacial cycles which occurred 2 Ma to 20 ka ago. Modern glacial ice and meltwaters are significantly depleted in ^{18}O, ranging from −40 to −18‰ $\delta^{18}O$ (e.g. Souchez et al., 1995, 1988; Mikucki et al., 2009; Claesson-Liljedahl et al., 2016). The isotopic composition of meltwater from Pleistocene ice sheets in Fennoscandia is estimated to have been −22 to −20‰ $\delta^{18}O$ (Pitkänen et al., 2004). An ice sheet over Britain would have had a similarly light isotopic composition. The observed isotopic composition of saline groundwaters in the basement rocks is heavier than this and is interpreted as a mixture of waters that have infiltrated at many different times and stages of glacial cycles during the Pleistocene period. Travel times from the surface for these groundwaters are therefore in the orders of 10^4–10^6 years, increasing with depth.

Brine samples in the deeper sedimentary cover rocks and the underlying basement rocks under the coast have heavier stable isotopic compositions than the other groundwater types, up to −5.1‰ $\delta^{18}O$, but the O and H isotope relationship indicates that these groundwaters also have a meteoric water origin but in a warmer climate than present-day (Bath et al., 2006). The most likely water source is infiltration to Triassic sedimentary rocks in the Irish Sea Basin during the Tertiary period when they were subaerially exposed in a sub-tropical climate prior to marine inundation. After infiltration, groundwater in the basin became saline by dissolution of evaporites in the Triassic sequence.

High $^{87}Sr/^{86}Sr$ ratios and high Br/Cl in saline groundwaters in basement rocks both suggest a greater extent of water-rock reaction and long residence times for these groundwaters (Bath et al., 2006). Lower Sr isotopic ratios in groundwaters in sedimentary cover rocks, especially in deep brines in the thick sedimentary sequence below the coast, probably result from the lower production of radiogenic ^{87}Sr in sandstones and in offshore evaporites from which the brines derive their high salinity.

A quantitative indication of how long the brines have resided in the deep sandstone and basement formations has been obtained from $^{36}Cl/Cl$ ratios (Metcalfe et al., 2007). $^{36}Cl/Cl$ ratios are mostly consistent with theoretical equilibrium values calculated from the concentrations of U and Th in rock obtained from natural gamma spectrometry logging. This indicates that Cl has been in these formations for at least 1.6 million years, and by implication that the bulk of the water in the brines is similarly old. Radiogenic helium (^4He) contents also indicate residence times for the brines of several million years, though there are few data and their water age interpretation involves various assumptions (Bath et al., 2006). Hydrodynamic modelling of brine movement across the Irish Sea basin eastwards towards the present coastline has suggested that travel times are 2–10 million years (Norris et al., 2007). There is broad consistency between the conclusions from modelling and interpretation of isotopic data that the brine contains Tertiary-age water.

The present-day water $\delta^{18}O$ depth profile, together with calculated isotopic values for calcite in equilibrium with present day groundwater conditions, are illustrated in Fig. 9a. These curves have been calculated using both the equations of Craig (1965) and Friedman and O'Neil (1977), taking account of the variation in temperature with depth. Where correlation of the $\delta^{18}O$ analyses with specific ME9 calcite growth zones was possible (section 4.5 and Supplementary Table S4) the outermost (i.e. most recent) calcite was found to have a $\delta^{18}O$ composition close to that predicted for calcite precipitating from the groundwater at the present day. However, much of the ME9 calcite is not in equilibrium with present-day groundwater conditions and has considerably more negative $\delta^{18}O$ values. Since the fluid inclusion observations (see below) show that ME9 represents low temperature mineralisation (< 80 °C), the very light stable isotopic compositions of the inner zones of ME9 calcite potentially indicate that cold-climate water containing a large contribution of glacial melt water.

As discussed above, it is reasonable to assume that the British Pleistocene ice sheets had a similar isotopic composition to that of Fennoscandia. Therefore, assuming a glacial water $\delta^{18}O$ value of −20‰$_{SMOW}$, theoretical $\delta^{18}O$ curves for calcite precipitated from present-day groundwater modified by the addition of 50% and 100% (volume) glacial water have been calculated in Fig. 9a. These modelled curves 'bracket' the most depleted $\delta^{18}O$ values found in the calcites and show that the bulk of the ME9 calcite analyses are consistent with precipitation in equilibrium with groundwaters containing between about 50% glacial component and groundwater with an isotopic composition consistent with recharge under temperate climate conditions similar to the present-day. Temperate climate recharge could have occurred during Pleistocene interglacials or during the Holocene). Some calcite values are more extreme, particularly in the upper part of the basement and base of the sandstone sequence (−390 to −800 m OD), and have values consistent with groundwater containing a larger component of glacial water. The very deepest sample of ME9 calcite (-1527 m in borehole 2) has a range of $\delta^{18}O$ consistent with precipitation from groundwater with up to 30% glacial component at some point during its growth history. Therefore, stable isotopic compositions of the inner growth zones of ME9 calcite indicate that cold climate water, including glacial melt water, circulated to > 1000 m depth in this part of the area. Pre-existing groundwaters in the east and central parts of the area were evidently displaced by the cold-climate, Pleistocene-age, water. This raises the question of what impact the groundwater movements had on redox conditions.

The palaeohydrogeology of this area from the Tertiary to the present is therefore dominated by the interactions of very old brine in the Triassic sedimentary sequence of the presently-offshore basin, almost

static due to its density and low hydraulic gradient, with onshore infiltration that has entered outcropping basement rocks and onlapping basin-edge sedimentary rocks and is driven by the topographic gradient. Isotopic compositions of the groundwaters and recorded within ME9 calcite associated with the modern groundwater system indicates that a large part of groundwater in the basement rocks has originated as infiltration during the many glacial and interglacial cycles through the Pleistocene.

Large scale permeability and hydraulic gradient have been sufficient to cause groundwater movement to at least 1000–1500 m depth in the central part of the area within the last 2 million years.

Groundwaters from these two distinct sources and ages converge and have mixed to produce saline groundwater in the basement rocks. Mixing is conceptualised as a dispersive hydrodynamic process where less dense infiltration 'skims' the top of more dense and immobile brine that penetrated from the basin to the deep basement over many millions of years.

The close association between the crystal morphology of the ME9 calcite and present-day groundwater salinities provides an insight into how the groundwater system has evolved over the Quaternary. The change of calcite morphology correlates with brackish groundwater chloride concentrations between 1000 and 2000 mg/L in the present zone of mixing at around 300 m depth. This change in calcite morphology and chemistry suggests that the ME9 calcite records groundwaters in this mixing zone having progressively evolved from saline to fresh/brackish during the Quaternary. The same evolution in calcite growth pattern is observed in boreholes across the area, although over a broader interval and shallower depths in the east, and over a narrower interval at greater depth in the west (boreholes 10A and 12A).

5.2. Palaeo-redox

Fe, Mn and Ce in the trace element compositions of ME9 calcite are interpreted as geochemical proxies for palaeo-redox. Co-genetic late-stage pyrite is an indicator of reducing conditions in the past, whilst iron and manganese oxyhydroxide minerals are indicators of oxidising conditions at the time of deposition.

Calibration of these geochemical proxies with data for present-day groundwaters and recently-formed ME9 calcite is incomplete because reliable Eh data are not available and there is some uncertainty over precisely which outer growth zones of ME9 are in equilibrium with present groundwater. Redox conditions in the present-day groundwaters are instead estimated on the basis of dissolved Fe. Groundwaters with relatively high (> 0.2 mg/L) Fe content are interpreted to be reducing and groundwaters with low contents (< 0.2 mg/L) are interpreted to be oxidising. The reducing/oxidising boundary for Fe solubility corresponds to an Eh range of about +150 to zero mV for a pH range of 7–8 (Appelo and Postma, 1993). As already noted, higher TDS and complexation also is a factor in Fe concentrations though redox is assumed to be the dominant factor here.

Ce concentrations are low in groundwater samples that are interpreted from Fe_{tot} to be oxidising, and conversely are higher in water samples that are interpreted to be reducing (Table 1). Ce concentrations are interpreted in the context of the dependence of $Ce^{3+}/Ce^{IV}O_2$ equilibrium on redox and pH. High dissolved Ce^{3+} is similar to Fe^{2+} in indicating reducing conditions but indicates more strongly reducing conditions as pH increases above 7. The Eh-pH diagram in Brookins (1989) indicates that the dissolved Ce^{3+} range of 10^{-9} to 10^{-7} M observed in these groundwaters (0.14–14 μg/L, Table 1) corresponds to an Eh range of about +100 to −200 mV for a range of pH 7 to 8.

From cathodoluminescence, a pattern of changes across the study area and over time in the Fe and Mn contents of growth zones in ME9 calcite from deeper fractures containing saline groundwaters has been established. Development of the growth zone sequence in ME9 calcite varies systematically from east to west across the site. The most complete sequence of zones is found in the boreholes from the east of the site, whereas calcites from the central area show intermediate numbers of zones and calcite from boreholes at the west of the site have a much-reduced sequence of zones. Iron sulphide mineralisation also decreases in abundance from east to west and is absent in the westernmost borehole (borehole 3). This progressive decrease in complexity of growth zoning from east to west and with increasing depth is consistent with a conceptual model whereby the flow system has evolved as meteoric infiltration in the east, progressively displacing older groundwaters as it moves westward and down-gradient. The eastern part of the area has experienced a longer period of meteoric infiltration and contains secondary calcite that records a longer history of groundwater flow and redox.

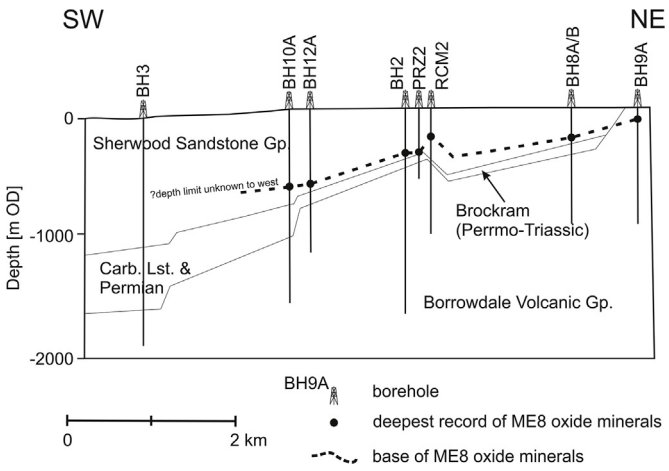

Fig. 11. Schematic cross-section showing the maximum depth of occurrence of ME8 manganese and iron oxyhydroxide minerals.

High Fe and Mn contents, indicated by CL and confirmed by microchemical analyses, for ME9 calcite below the MTZ indicate that reducing conditions prevailed at the time of precipitation. Variations of Fe and Mn contents (Fig. 6 and Supplementary Table S3) between CL zones of ME9 suggest that the strength of reducing conditions and/or the salinity fluctuated through time. It is concluded that reducing conditions persisted, though with varying strength, through the period of ME9 precipitation. Traces of Fe sulphide in some calcite growth zones support this interpretation and indicate from Fe-S equilibria that Eh was around −200 ± 50 mV. There are alternative geochemical models that could link varying Fe contents of secondary calcite to redox. For example, low-Fe calcite might have formed due to sulphate reduction and Fe sulphide precipitation lowering Fe^{2+} concentrations in the calcite (since Fe^{2+} is preferentially precipitated in sulphide in the presence of S^{2-}).

Lower Fe and Mn contents are found in above-MTZ ME9 calcite (Fig. 7). Growth zones in shallow ME9 calcites, identified by their varying luminescence, cannot be correlated between fractures and seem to record localised variations in the geochemical environment. The overall evolution of the zoning towards dominantly non-ferroan, non-manganoan calcite suggests that groundwater at these depths may have become more oxidising with time during growth of the calcite.

Manganese and iron oxyhydroxides are mostly attributed to the ME8 mineralisation episode and are related to oxidative dissolution of pre-existing ferro-manganoan carbonate fracture mineralisation and similar carbonate cements in the sandstone aquifer. Limited ^{40}Ar-^{39}Ar ages of potassium-rich manganese oxyhydroxide indicates (14–21 Ma: Table 4), show that it extends back as far as the late-Tertiary. It is attributed primarily to supergene (weathering) processes following Miocene uplift (Chadwick et al., 1993, 1994; Holliday, 1993; Milodowski et al., 1998) and continues today. Fig. 11 summarises the maximum depth limit to which late-stage ME8 Mn-Fe oxyhydroxide mineralisation is present in fractures in the deep boreholes from northeast to

southwest across the study area. The distribution of ME8 Mn-Fe oxyhydroxide suggests that, during the Tertiary period, oxidising groundwaters penetrated in some locations to greater depths than oxic groundwaters do at present. The absence of ME8 Mn-Fe oxyhydroxides from basement rock under sedimentary cover (Fig. 11), however, suggests that the lower permeability mudstones, muddy sandstones and muddy breccias of the Brockram, St Bees Shale, and basal part of St Bees Sandstone at the base of the sedimentary sequence have been the limit of oxidising groundwaters since the Tertiary. The only hematite that occurs in basement rock is attributed to much earlier (Mesozoic and Palaeozoic) hydrothermal mineralisation (Milodowski et al., 1998).

Late-stage Mn-Fe oxyhydroxide, occurring with c-axis shortened ME9 calcite, occurs only in the upper parts of the aquifer sandstone to between 270 and 440 m depth, in the central part of the area, and up to ~660 m depth further west in boreholes 10A and 12A, where current groundwaters are dilute or brackish (Milodowski et al., 1997, 1998). Further east, it occurs to a maximum depth of 150 m in the fractured BVG in borehole 8A and 25 m in borehole 9A. It indicates that oxidising conditions in these relatively shallow groundwaters have probably persisted for the duration of the Quaternary period.

There is a strong negative Ce anomaly in REE analyses of above-MTZ ME9 calcites (Fig. 8a and Table 3). Ce is depleted by up to three orders of magnitude relative to LREE in youngest non-luminescent growth zones. In contrast, older luminescent growth zones do not show a Ce anomaly. The time-dependent change from non-luminescent Ce-depleted calcite to luminescent uniform-REE calcite coincides with a change of morphology from c-axis flattened to c-axis elongated. These changes are interpreted to indicate a temporal change from reducing saline to oxidising dilute groundwater conditions in the shallow part of the system.

A negative Ce anomaly is not found in ME9 calcite from below −250 m OD, i.e. in below-MTZ type calcite, is further evidence supporting the interpretation that reducing conditions, i.e. more negative than +100 to −200 mV depending on pH, have persisted in the deeper groundwaters.

The fact that a negative Ce anomaly is found only in the outer growth zones of calcite samples from −250 m OD (Table 3; Figs. 6 and 9), whereas ME9 calcites from deeper fractures do not show the anomaly, suggests that redox variation affecting Ce solubilities has occurred only at this relatively shallow depth in the timescales represented by the growth of the calcite samples, i.e. probably through the Quaternary period based on the $^{230}Th/^{234}U$ radiometric ages obtained for the calcite (Table 4).

5.3. Conceptual model for palaeohydrogeology and palaeo-redox

Palaeohydrogeology of the groundwater system in west Cumbria has been determined by a number of factors.

Topography west of the study area evolved by inversion of the East Irish Sea Basin and erosion of much of the Mesozoic sequence so that from the Tertiary onwards the present-day seabed area has comprised mostly Triassic sedimentary rocks overlain since the Pleistocene by a thin veneer of glacial sediments. Topography east of the study area has been dominated by the Cumbrian mountains which are outcrops of basement rocks and therefore more resistant to erosion. Large scale topographic gradient westwards of the hills would have been greatest during the Tertiary, when the present-day Irish Sea area was sub-aerial.

Evaporites in the thick, halite-bearing Mercia Mudstone Group (upper Triassic) sedimentary sequence offshore are the source and buffer for halite-saturated brines in the basin. In the Tertiary period, and possibly more recently at interglacial stages of the Pleistocene, brines were formed by westwards flow of groundwater through permeable Triassic sandstones and dissolution of halite in the basin.

During the Quaternary, brine from the basin migrated eastwards into the study area and was diluted to produce groundwaters with varying salinities and densities which have an important influence on groundwater hydraulics at depth in the study area. The inferred reversal of flow directions at the start of the Pleistocene was probably related to changes of isostatic sea level and to restrictions of infiltration during periglacial and glacial climate stages.

In the Pleistocene, there were several glacial stages during which the study area would have been covered by many hundreds of metres of ice. Ice sheets might have restricted infiltration due to basal freezing for parts of those episodes, whilst in other periods there would have been enhanced infiltration of meltwater due to the sub-glacial water pressures related to the overlying ice load. There would also have been longer periods of periglacial conditions during which permafrost restricted infiltration. There are large uncertainties in the understanding and quantitative modelling of sub-glacial and sub-permafrost groundwater movements. Several lines of evidence described above indicate that the cumulative impact of these glacial processes in the study area has not substantially disrupted the groundwater system and that the arrangement of flow regimes controlled by permeabilities and water salinities has not varied significantly through the Quaternary period.

Sea level changes, eustatic and isostatic, occurred during the Quaternary. The present location of the coast close to the study area was established in the late Pleistocene as Devensian glaciation receded and sea level rose. Shallow fresh groundwater flow westwards through the sandstones is diverted upwards at the interface with intruded seawater. The position of the coastline, along with surface topography, permeabilities of underlying rocks, and vertical distribution of groundwater salinity have together controlled movements and mixing of groundwaters in the study area.

It follows from the relative stability of physical hydrogeology and the major influence for many millions of years of evaporite-derived salinity that groundwater compositions have also remained fairly constant through the Quaternary. Varying fresh meteoric infiltration through the Quaternary, as at present, is coupled with the introduction of dissolved oxygen at the top of the groundwater system and the associated effects on redox conditions.

Mineralogical evidence suggests that oxidising groundwater persists in the sandstones to variable depths but does not penetrate beyond the base of the sedimentary rocks into the BVG basement. The combined results from the occurrence and distribution of secondary pyrite and iron and manganese oxides, and from the Fe, Mn and REEs contents of secondary calcites suggest overall that palaeo-redox conditions were oxidising to about 250–300 m depth at some time in the past. This is probably deeper than at present. Mineral sources of Fe(II) and Mn consume dissolved oxygen and produce late stage Fe and Mn oxyhydroxides which are restricted to that depth interval. Geochemical proxies indicate that redox conditions in the deeper sedimentary sequence and in basement groundwaters might have had relatively minor fluctuations whilst overall remaining reducing. Isotopically light $\delta^{18}O$ in both groundwaters and ME9 calcite indicates that Pleistocene-age groundwaters, some of which would have originated as glacial meltwater, have penetrated the basement to at least 700 m depth. The very long groundwater travel times, up to 10^6 years, to the deeper sampled points in the basement are consistent with the very low permeabilities inferred from the preservation of relic sub-glacial groundwater pressures (Black and Barker, 2015). The fact that the ME9 calcite in the sedimentary strata below 250–300 m and underlying basement rocks is ferromanganoan and shows no Ce anomaly demonstrates that these groundwaters were no longer oxidising by the time they reached these depths. These observations are consistent with other studies in glaciated fractured crystalline terrain and experimental studies, which show that the rock mass is able to effectively remove dissolved oxygen from glacial meltwater at shallow depths (0–300 m), by reaction with reduced Fe and Mn minerals, and buffer redox to reducing conditions (e.g. Puigdomenech et al., 2001; Drake et al., 2009, 2017; Claesson-Liljedahl et al., 2016).

6. Summary and conclusions

A portfolio of methods has been applied to groundwater and rock samples from boreholes in the study area to elucidate the past evolution of the groundwater system in basement rocks and sedimentary cover rocks. Of particular interest are the response of groundwater conditions to external climate-driven variables, the degree to which resulting changes are attenuated with depth, and what are the hydrogeological and other characteristics of the area that influence palaeohydrogeology.

Interpretations of hydrochemical and isotopic data for groundwaters have already been published. They described the groundwater system in fractured meta-volcanic basement rock overlain by a sedimentary sequence. The area is located on the west Cumbrian coastal plain at Sellafield. The conceptual model of groundwater movements based on hydrogeological and hydrochemical interpretations is composed of three regimes with contrasting hydrodynamics and groundwater ages. The two deeper regimes comprise: (i) groundwater movement westwards through basement and bottom of the overlying sedimentary rocks, driven by infiltration and topographic gradient, becoming saline and having isotopic indication of water ages > 10 ka, and (ii) brine groundwaters that have intruded into underlying basement from the offshore sedimentary basin and that move very slowly on the evidence of isotopic residence times > 1.5 Ma.

This paper describes how the conceptual model for the past evolution of the groundwater system at Sellafield can be enhanced by use of mineralogical information. Interpretation of data for secondary minerals has been focussed on understanding the salinity and redox conditions of past groundwaters.

Secondary calcites have been characterised by morphology, stable isotope analyses, radioactive dating, cathodoluminescence, and microanalyses of iron, manganese and REEs. The information interpreted from these are, respectively, groundwater salinity, origin of groundwater, age of calcite precipitation, and redox conditions during calcite precipitation.

External morphology of the youngest generation of secondary calcite (ME9) correlates with salinity (TDS) of co-existing present-day groundwater. Morphology of older growth zones inside calcite crystals is interpreted as an indication of past groundwater salinities. It indicates that the upper part of the groundwater system has become more dilute over time. Meteoric water infiltration, possibly enhanced by post-glacial land uplift, has been slowly flushing out pre-existing groundwater that had become brackish/saline by dispersive mixing with much deeper groundwater over a timescale corresponding to the period of glacial climate cycles, i.e. about 2 Ma.

Stable oxygen isotopic compositions of calcite growth zones have a wide range of values. They range from values close to equilibrium with present-day groundwater to more negative values that represent precipitation from groundwater with a substantial component of glacial melt water. Groundwater flowing to more than 700 m depth in the centre of the area had a greater contribution from glacial melt water than does present-day groundwater. However, calcite morphologies indicate that the associated flushing did not reach a high level of dilution (< 300 mg/L TDS).

Radiometric Th-U ages for calcites give ages in the order of 10^4-10^5 a. These support the interpretation of calcite having precipitated from groundwaters during the Quaternary period, i.e. from the present back to about 2×10^6 years ago. A single age by an improved Th-U method is greater at 10^7 a and could be accounted for by the sample for that analysis coming from the calcite core whereas other analyses were on samples from outer, i.e. younger, growth zones.

Cathodoluminescence (CL) images and microanalyses indicate that calcite growth zones contain varying concentrations proportions of Fe and Mn. The patterns of variation change with depth, i.e. between dilute and brackish/saline groundwaters. Fe contents in calcite zones as seen in CL are interpreted as a proxy for redox conditions in groundwaters at the time of growth. Variability within higher Fe contents probably indicates fluctuations of the other redox-active variables such as sulphide, as well as Fe mineral sources and groundwater salinity.

High dissolved Ce^{3+} is another proxy indicator of reducing conditions. It discriminates over a different range of Eh than Fe^{2+}, taking into account the respective pH dependences. Oxidation of Ce and depletion in solution occurs at moderately negative Eh (e.g. −200 mV at pH 8). Relatively high Ce content in calcite indicates that co-existing groundwater was reducing. REEs in outer growth zones of calcites from shallow dilute groundwater have distinctive chondrite-normalised REE patterns with a negative Ce anomaly indicating oxidising conditions, whereas this is absent in calcites from greater depth where groundwaters are saline. The absence of a negative Ce anomaly indicates that reducing conditions prevailed in deeper groundwaters at the time of calcite precipitation.

Salinities of fluid inclusions from the inner, older, zones of calcite from the centre of the area generally increase with depth, similarly to the distribution of present groundwater salinities. Higher groundwater salinities in the early Quaternary or the Miocene periods are consistent with the palaeohydrogeological concept that brines intruded further eastwards, from the basin into the basement and deeper part of the sedimentary sequence, than it does at present.

Distributions of iron oxyhydroxide minerals and pyrite are evidence at a larger scale of whether groundwater redox might have undergone major change, i.e. reducing to oxidising, as the groundwater system has evolved to its present state. Iron and manganese oxyhydroxides are found only in the relatively-shallow sandstone in the centre of the area. coinciding with dilute groundwater. Fine-grained pyrite is found between growth zones in secondary calcite in the basement and at the base of the sandstone, and as fracture coatings in basement rock. Persistence of pyrite indicates that reducing conditions have been sustained at these depths.

There are no indications from these mineralogical and mineral chemistry proxies of redox that oxidising groundwater penetrated beyond the sedimentary cover rock during the Quaternary. Although cold-climate water, including episodic glacial melt water recharge, penetrated to several hundreds of metres depth in the basement rocks in the centre of the area, dissolved oxygen had been removed by water-rock reaction. Redox fluctuated within a range of reducing conditions that have varying controls by the Fe, S and C redox couples, probably in conjunction with the groundwater movements described above.

Integrating the findings from these mineralogical and geochemical investigations improves knowledge of past salinity and redox changes in deep (> 200 m) groundwaters of the Sellafield area in northwest England. Data, processes and interpretations relate dominantly to the Quaternary period, between 2 Ma ago and present. There is interest in how deep groundwater conditions changed as surface and shallow environments were affected by glacial and interglacial cycles. Glacial melt water displaced groundwater to ~700 m depth in episodes during those cycles. Those Pleistocene groundwaters have in turn been substantially dispersed and mixed with groundwaters with dominantly temperate climate origins. Prior to these Pleistocene episodes, levels of salinity in basement groundwaters were probably higher and more directly influenced by the offshore sedimentary basin. The lithological change from cover sedimentary sequence to basement rocks has continued to be a significant hydrogeological boundary as indicated by the transition in the centre of the area from dilute to brackish/saline waters which has shifted downwards over time due to freshening by infiltrating meteoric water.

This study shows how characterisation of secondary minerals can contribute to palaeohydrogeology, i.e. the knowledge of past groundwater conditions. Interpretations of data from minerals supplement interpretations of groundwater evolution from data for groundwater compositions and environmental isotopes. The information gained for palaeohydrogeology is qualitative or semi-quantitative as also is the timescale for episodes and changes through the Quaternary. The information makes significant contributions that constrain the breadth of

alternative concepts for how deep groundwater movements and chemical conditions have evolved in response to the climatic and hydrological changes at the surface boundary through the last 2 Ma. It has application, for example, to the calibration of a numerical palaeohydrogeological model of how the groundwater system has evolved from past to present, and from present into the future.

Acknowledgements

The work presented here summarises investigations initially undertaken on behalf of United Kingdom Nirex Limited as part of a programme of site investigations at Sellafield, with subsequent research funded under the European Commission 4th Framework EQUIP (Contract No. FI4W-CT96-0031) and 5th Framework PADAMOT (Contract No. FIKW-CT2001-20129) projects, and by the British Geological Survey (BGS). This paper was funded by Radioactive Waste Management Limited. It represents a team effort involving the scientific input and support of many other colleagues at the British Geological Survey, and by EQUIP and PADAMOT project partners. The authors would also like to thank staff at the NERC Isotope Geoscience Laboratory (NIGL) and Scottish Universities Environmental Research Centre (SUERC) for undertaking the stable and radiogenic isotope analyses. In particular, the authors acknowledge the valuable contributions made by M.R. Gillespie (BGS), Jon Bouch (BGS), S.R.N. Chenery (BGS), T.J. Shepherd (BGS), J Naden (BGS), H Sloane (NIGL) and C. Chenery (NIGL). N Roberts (NIGL) is thanked for kindly allowing us to quote the unpublished U-Pb age information obtained by LA-PIMMS from one of our calcite samples. We also thank Dr E-L Tullborg and two anonymous reviewers for their well-considered and constructive comments, which greatly improved the manuscript. AEM publishes with the permission of the Executive Director of the British Geological Survey (NERC).

Appendix A. Supplementary data

Supplementary data related to this article can be found at https://doi.org/10.1016/j.apgeochem.2018.07.008.

References

Akhurst, M.C., Chadwick, R.A., Holliday, D.W., McCormac, M., McMillan, A.A., Millward, D., Young, B., 1997. Geology of the West Cumbria District, vol. 28. British Geological Survey Memoir, England and Wales, Sheets, Whitehaven, pp. 37 (Gosforth) and 47 (Bootle).

Appelo, C.A.J., Postma, D., 1993. Geochemistry, Groundwater and Pollution, first ed. A.A. Balkema, Rotterdam.

Astilleros, J.M., Pina, C.M., Fernández-Díaz, L., Putnis, A., 2002. Molecular-scale surface processes during the growth of calcite in the presence of manganese. Geochem. Cosmochim. Acta 66, 3177–3189.

Barclay, W.J., Riley, N.J., Strong, G.E., 1994. The Dinantian rocks of the Sellafield area, west Cumbria. Proc. Yorks. Geol. Soc. 50, 37–49.

Barnaby, R.J., Rimstidt, J.D., 1989. Redox conditions of calcite cementation interpreted from Mn and Fe contents of authigenic calcites. Geol. Soc. Am. Bull. 101, 795–804.

Bath, A.H., McCartney, R.A., Richards, H.G., Metcalfe, R., Crawford, M.B., 1996. Groundwater chemistry in the Sellafield area: a preliminary interpretation. Q. J. Eng. Geol. 29, S39–S57.

Bath, A., Milodowski, A.E., Ruotsalainen, P., Tullborg, E.-L., Cortés Ruiz, A., Aranyossy, J.-F., 2000. Evidence from Mineralogy and Geochemistry for the Evolution of Groundwater Systems during the Quaternary for Use in Radioactive Waste Repository Safety Assessment (EQUIP Project). Report EUR 19613. D-G for Research, European Commission, Brussels.

Bath, A., Richards, H., Metcalfe, R., McCartney, R., Degnan, P., Littleboy, A., 2006. Geochemical indicators of deep groundwater movements at Sellafield, UK. J. Geochem. Explor. 90, 24–44.

Black, J.H., Barker, J.A., 2015. The puzzle of high heads beneath the West Cumbrian coast, UK: a possible solution. Hydrogeol. J. https://doi.org/10.1007/s10040-015-1340-4.

Black, J.H., Brightman, M.A., 1996. Conceptual model of the hydrogeology of the Sellafield area. Q. J. Eng. Geol. 29, S83–S94.

Bouch, J.E., Milodowski, A.E., Ambrose, K., 2004. Contrasting patterns of pore-system modification due to dolomitization and fracturing in Dinantian basin-margin carbonates from the UK. In: In: Braithwaite, C.J.R., Rizzi, G., Darke, G. (Eds.), The Geometry and Petrogenesis of Dolomite Hydrocarbon Reservoirs, vol. 235. Geological Society of London, Special Publication, pp. 325–348.

Braun, J.-J., Pagel, M., Muller, J.-P., Bilong, P., Michard, A., Guillet, B., 1990. Cerium anomalies in lateritic profiles. Geochem. Cosmochim. Acta 54, 781–795.

Brookins, D.G., 1989. Aqueous geochemistry of rare earth elements. Rev. Mineral. Geochem. 21, 201–225.

Chadwick, R.A., Evans, D.J., Holliday, D.W., 1993. The Maryport Fault: the post-Caledonian tectonic history of southern Britain in microcosm. Journal of the Geological Society, London 150, 247–250.

Chadwick, R.A., Kirby, G.A., Bailey, H.E., 1994. The post-Triassic structural evolution of north-west England and adjacent parts of the East Irish Sea. Proc. Yorks. Geol. Soc. 50, 91–102.

Claesson-Liljedahl, L., Kontula, A., Harper, J., Näslund, J.-O., Selroos, J.-O., Pitkänen, P., Puigdomenech, I., Hobbs, M., Follin, S., Hirschorn, S., Jansson, P., Kennell, L., Marcos, N., Ruskeeniemi, T., Tullborg, E.-L., Vidstrand, P., 2016. The Greenland Analogue Project: Final Report. SKB Technical Report, TR-14–13. Svensk Kärnbränslehantering AB, Stockholm, Sweden.

Clark, C.D., Gibbard, P.L., Rose, J., 2004. Pleistocene glacial limits in England, Scotland and Wales. In: Elhers, J., Gibbard, P.L. (Eds.), Quaternary Glaciations—extent and Chronology. Part I: Europe. Elsevier, Amsterdam.

Colter, V.S., Barr, K.W., 1975. Recent developments in the geology of the Irish sea and Cheshire basins. In: Woodland, A.W. (Ed.), Petroleum and the Continental Shelf of NW Europe. Applied Science, London, pp. 61–73.

Craig, H., 1965. The measurement of oxygen isotope paleotemperatures. In: Tongiorgi, E. (Ed.), Stable Isotopes in Oceanographic Studies and Paleotemperatures. Proceedings of the Spoleto Conference. Consiglio Nazionale delle Ricerche, Pisa, pp. 3–24.

Crowley, S.F., Bottrell, S.H., McCarthy, M.D.B., Ward, J., Young, B., 1997. $\delta^{34}S$ of Lower Carboniferous anhydrite, Cumbria and its implications for barite mineralization in the northern Pennines. J. Geol. Soc. 154, 597–600.

Davis, K., Dove, P., Wasylenki, L., De Yoreo, J.J., 2015. Morphological consequences of differential Mg^{2+} incorporation at structurally distinct steps on calcite. Am. Mineral. 89, 714–720.

Dickson, J.A.D., 1966. Carbonate identification and genesis as revealed by staining. J. Sediment. Petrol. 36, 491–505.

Drake, H., Tullborg, E.-L., 2009. Paleohydrogeological events recorded by stable isotopes, fluid inclusions and trace elements in fracture minerals in crystalline rock, Simpevarp area, SE Sweden. Appl. Geochem. 24, 715–732.

Drake, H., Tullborg, E.-L., MacKenzie, A.B., 2009. Detecting the near-surface redox front in crystalline bedrock using fracture mineral distribution, geochemistry and U-series disequilibrium. Appl. Geochem. 24, 1023–1039.

Drake, H., Åström, M.E., Heim, C., Broman, C., Åström, J., Whitehouse, M.J., Ivarsson, M., Siljeström, S., Sjövall, P., 2015. Extreme ^{13}C-depletion of carbonates formed during oxidation of biogenic methane in fractured granite. Nat. Commun. 6 (7020), 9.

Drake, H., Suksi, J., Tullborg, E.-L., Lahaye, Y., 2017. Quaternary redox transitions in deep crystalline rock fractures at the western margin of the Greenland ice sheet. Appl. Geochem. 76, 196–209.

Fletcher, B.N., Ransome, C.R., 1978. Offshore Cumbria. In: Mosely, F. (Ed.), The. Geology of the Lake District, vol. 3. Yorkshire Geological Society Occasional Publication, pp. 242–249.

Folk, R.L., 1974. The natural history of crystalline calcium carbonate: effect of magnesium content and salinity. J. Sediment. Petrol. 44, 40–53.

Friedman, I., O'Neil, J.R., 1977. Compilation of Stable Isotope Fractionation Factors of Geochemical Interest. U.S. Geological Survey, pp. KK1–KK12 Professional Paper, 440-KK.

Given, R.K., Wilkinson, B.H., 1985. Kinetic control on morphology, composition and mineralogy of abiotic sedimentary carbonates. J. Sediment. Petrol. 55, 109–119.

Gonzalez, L.A., Carpenter, S.C., Lomann, K.C., 1992. Inorganic calcite morphology: roles of fluid chemistry and fluid flow. J. Sediment. Petrol. 62, 382–399.

Guimerà, J., Duro, L., Jordana, S., Bruno, J., 1999. Effects of Ice Melting and Redox Front Migration in Fractured Rocks of Low Permeability. SKB Technical Report, TR-99–19. Svensk Kärnbränslehantering AB, Stockholm, Sweden.

Gutmanis, J.C., Lanyon, G.W., Wynn, T.J., Watson, C.R., 1998. Fluid flow in faults: a study of fault hydrogeology in Triassic sandstone and Ordovician volcaniclastic rocks at Sellafield, north-west England. Proc. Yorks. Geol. Soc. 52, 159–175.

Heathcote, J.A., Michie, U.McL., 2004. Estimating hydrogeological conditions over the last 120 ka: an example from the Sellafield area. Journal of the Geological Society, London 161, 995–1008.

Holliday, D.W., 1993. Mesozoic cover over northern England: interpretation of apatite fission track data. Journal of the Geological Society, London 150, 657–660.

Humphris, S.E., 1984. The mobility of the rare earth elements in the crust. In: Henderson, P. (Ed.), Rare Earth Element Geochemistry, Developments in Geochemistry Series, 2. Elsevier, Amsterdam, pp. 317–342.

Kimbell, T.N., Humphrey, J.D., 1994. Geochemistry and crystal morphology of aragonite cements of mixing-zone origin, Barbados, West Indies. J. Sediment. Res. A64, 604–614.

Korte, C., Kozur, H.W., Bruckschen, P., Veitzer, J., 2003. Strontium isotope evolution of late permian and triassic seawater. Geochem. Cosmochim. Acta 67, 47–62.

Lahann, R.W., 1978. A chemical model for calcite crystal growth and morphology control. J. Sediment. Petrol. 48, 337–344.

Leybourne, M.I., Goodfellow, W.D., Boyle, D.R., Hall, G.M., 2000. Rapid development of negative Ce anomalies in surface waters and contrasting REE patterns in groundwaters associated with Zn-Pb massive sulphide deposits. Appl. Geochem. 15, 695–723.

Machel, H.G., Burton, E.A., 1991. Factors governing cathodoluminescence in calcite and dolomite, and their implications for studies of carbonate diagenesis. In: In: Barker, C.E., Kopp, O.C. (Eds.), Luminescence Microscopy: Quantitative and Qualitative Aspects, vol. 25. SEPM (Society for Sedimentary Geology) Short Course, pp. 37–57.

Marshall, J.D., 1988. Cathodoluminescence of Geological Materials. Allen & Unwin Inc, USA.
McArthur, J.M., Howarth, R.J., Bailey, T.R., 2001. Strontium isotope stratigraphy: LOWESS Version 3: best fit to the marine Sr-isotope curve for 0–509 Ma and accompanying look-up table for deriving numerical age. J. Geol. 109, 155–170.
McEvoy, F.M., Schofield, D.J., Shaw, R.P., Norris, S., 2016. Tectonic and climatic considerations for deep geological disposal of radioactive waste: a UK perspective. Sci. Total Environ. 571, 507–521.
McLennan, S.M., 1989. Chapter 7. Rare earth elements in sedimentary rocks: influence of provenance and sedimentary processes. In: In: Lipin, B.R., McKay, G.A. (Eds.), Geochemistry and Mineralogy of Rare Earth Elements. Reviews in Mineralogy, vol. 21. Mineralogical Society of America, Washington, D.C, pp. 169–200.
Metcalfe, R., Crawford, M.B., Bath, A.H., Littleboy, A.K., Degnan, P.J., Richards, H.G., 2007. Characteristics of deep groundwater flow in a basin marginal setting at Sellafield, Northwest England: ^{36}Cl and halide evidence. Appl. Geochem. 22, 128–151.
Michie, U.McL., 1996. The geological framework of the Sellafield area and its relationship to hydrogeology. Q. J. Eng. Geol. 29, S13–S28.
Michie, U. McL., Bowden, R.A., 1994. UK NIREX geological investigations at Sellafield. Proc. Yorks. Geol. Soc. 50, 5–9.
Mikucki, J.A., Pearson, A., Johnston, D.T., Turchyn, A.V., Farquhar, J., Schrag, D.P., Anbar, A.D., Priscu, J.C., Lee, P.A., 2009. A contemporary microbially maintained subglacial ferrous "ocean". Science 397–400.
Milodowski, A.E., Gillespie, M.R., Shaw, R.P., Bailey, D.E., 1995. Flow-zone Characterisation: Mineralogical and Fracture Orientation Characteristics in the PRZ and Fleming Hall Fault Zone Area Boreholes. Sellafield. Nirex Report, SA/95/001. United Kingdom Nirex Limited, Harwell, Oxfordshire, UK.
Milodowski, A.E., Barnes, R.P., Phillips, E.R., Shaw, R.P., 1997. Summary Data Compilation for the Location, Distribution and Orientation of Potential Flowing Features in the Sellafield Boreholes. Nirex Report, SA/97/031. United Kingdom Nirex Limited, Harwell, Oxfordshire, UK.
Milodowski, A.E., Gillespie, M.R., Naden, J., Fortey, N.J., Shepherd, T.J., Pearce, J.M., Metcalfe, R., 1998. The petrology and paragenesis of fracture mineralization in the Sellafield area, west Cumbria. Proc. Yorks. Geol. Soc. 52, 215–241.
Milodowski, A.E., Fortey, N.J., Gillespie, M.R., Pearce, J.M., Hyslop, E.K., 2002. Synthesis Report on the Mineralogical Characteristics of Fractures from the Nirex Boreholes in the Sellafield Area. British Geological Survey, Technical Report, WG/98/8. .
Milodowski, A.E., Tullborg, E.-L., Buil, B., Gómez, P., Turrero, M.-J., Haszeldine, S., England, G., Gillespie, M.R., Torres, T., Ortiz, J.E., Zachariáš, Silar, J., Chvátal, M., Strnad, L., Šebek, O., Bouch, J.E., Chenery, S.R., Chenery, C., Shepherd, T.J., Mckervey, J.A., 2005. Application of Mineralogical, Petrological and Geochemical Tools for Evaluating the Palaeohydrogeological Evolution of the PADAMOT Study Sites. PADAMOT Project Technical Report, WP2, EU FP5 CONTRACT NO. FIKW-CT2001-20129. United Kingdom Nirex Limited, Harwell, Oxfordshire, UK.
Mozley, P., Burns, S.J., 1993. Oxygen and carbon isotope comparison of marine carbonate concretions: an overview. J. Sediment. Petrol. 63, 73–83.
Myers, W.J., 1991. Calcite cement stratigraphy: an overview. In: In: Barker, C.E., Kopp, O.C. (Eds.), Luminescence Microscopy: Quantitative and Qualitative Aspects, vol. 25. SEPM (Society for Sedimentary Geology) Short Course, pp. 133–149.
Naden, J., 1996. CalcBrine 1.5: a Microsoft Excel 5.0 Add-in for Calculating Salinities from Microthermometric Data in the System NaCl-cacl$_2$-h2o. PACROFI VI Abstracts. University of Winsconsin.
Nirex, 1997a. An Assessment of the post-closure Performance of a Deep Waste Repository at Sellafield. Volume 1: Hydrogeological Model Development – Conceptual Basis and Data. UK Nirex Ltd. Report, S/97/012. United Kingdom Nirex Limited, Harwell, Oxfordshire, UK.
Nirex, 1997b. Hydrochemistry of Sellafield: 1997 Update. Sellafield Geological and Hydrogeological Investigations. Nirex Science Report, SA/97/089. UK Nirex Ltd, Harwell, Oxfordshire, UK.
Nirex, 1997c. Locations of Flow Zones in Sellafield Boreholes. UK Nirex Ltd Report, SA/97/036. United Kingdom Nirex Limited, Harwell, Oxfordshire, UK.
Nirex, 1998a. Constraining the Timing of Movements on Sellafield Faults. UK Nirex Ltd Report, SA/97/033. United Kingdom Nirex Limited, Harwell, Oxfordshire, UK.
Nirex, 1998b. Sellafield Geological and Hydrogeological Investigations. Compilation of Reconnaissance Studies for Selected Isotope, Gas and Trace Element Data from Sellafield. Sellafield Geological and Hydrogeological Investigations. Nirex Science Report, SA/97/090. UK Nirex Ltd, Harwell, Oxfordshire, UK.
Norris, S., Breen, B., Knight, L., 2007. Use of geoscientific arguments in the Nirex Phased Geological Repository concept: illustrative desk study. In: Linkage of Geoscientific Arguments and Evidence in Supporting the Safety Case. Proceedings of Second AMIGO Workshop, Toronto, Sept 2005. Nuclear Energy Agency, Paris, pp. 155–156.
Parker, S.C., Titiloye, J.O., Watson, W., 1993. Molecular modelling of carbonate minerals: studies of growth and morphology. Philosophical Transactions of the Royal Society A344, 37–48.
Pitkänen, P., Partamies, S., Luukkonen, A., 2004. Hydrogeochemical Interpretation of Baseline Groundwater Conditions at the Olkiluoto Site. Posiva Report 2003-07. Posiva Oy, Olkiluoto, Finland.
Puigdomenech, I., Ambrosi, J.-P., Eisenlohr, L., Lartigue, J.-E., Banwart, S.A., Bateman, K., Milodowski, A.E., West, J.M., Griffaut, L., Gustafsson, E., Hama, K., Yoshida, H., Kotelnikova, S., Pedersen, K., Michaud, V., Trotignon, L., Rivas Perez, J., Tullborg, E.-L., 2001. O_2 Depletion in Granitic media: the REX Project. SKB Technical Report, TR-01–05. Svensk Kärnbränslehantering AB, Stockholm, Sweden.
Roedder, E., 1984. Fluid inclusions. Mineralogical Society of America. Rev. Mineral. 12.
Roberts, N.W., Walker, R.J., 2016. U-Pb geochronology of calcite mineralized faults; absolute dating of rift-related fault events on the northeast Atlantic margin. Geology 44, 531–534.
Savard, M.M., Veizer, J., Hinton, R., 1995. Cathodoluminescence at low Fe and Mn concentrations: a SIMS study of zones in natural calcites. J. Sediment. Res. A65, 208–213.
Schmidt, V., McDonald, D.A., 1979. The role of secondary porosity in the course of sandstone diagenesis. In: In: Scholle, P.A., Schluger, P.R. (Eds.), *Aspects of Diagenesis*, Society of Economic Paleontologists and Mineralogists, vol. 26. Special Publication, pp. 175–207.
Souchez, R., Lemmens, M., Chappellaz, J., 1995. Flow-induced mixing in the GRIP basal ice deduced from the CO_2 and CH_4 records. Geophys. Res. Lett. 41–44 March 1995.
Souchez, R., Lorrain, R., Tison, J.L., Jouzel, J., 1988. CO-isotopic signature of two mechanisms of basal-ice formation in Arctic outlet glaciers. Ann. Glaciol. 10, 163–166.
Stauffer, B., Neftel, A., Oeschger, H., Schwander, J., 1985. CO_2 concentration in air extracted from Greenland ice samples. In: In: Langway, C.C., Oeschger, H., Dansgaard, W. (Eds.), Greenland Ice Core: Geophysics, Geochemistry and the Environment, vol. 33. American Geophysical Union, Geophysical Monograph, pp. 85–89.
Strong, G.E., Milodowski, A.E., Pearce, J.M., Kemp, S.J., Prior, S.V., Morton, A.C., 1994. The petrology and diagenesis of Permo-Triassic rocks of the Sellafield area, Cumbria. Proc. Yorks. Geol. Soc. 50, 77–89.
Temman, M., Paquette, J., Vali, H., 2000. Mn and Zn incorporation into calcite as a function of chloride aqueous concentration. Geochem. Cosmochim. Acta 64, 2417–2430.
Vasconcelos, P.M., Renne, P.R., Brimhall, G.H., Becker, T.A., 1994. Direct dating of weathering phenomena by ^{40}Ar/^{39}Ar and K-Ar analysis of supergene K-Mn oxides. Geochem. Cosmochim. Acta 58, 1635–1665.